Article:
Meng, Q, Xue, W, Chen, F et al. (2022) Stratigraphy of the Guadalupian (Permian) siliceous deposits from central Guizhou of South China: Regional correlations with implications for carbonate productivity during the Middle Permian biocrisis. Earth-Science Reviews, 228. 104011. ISSN: 0012-8252

https://doi.org/10.1016/j.earscirev.2022.104011

Stratigraphy of the Guadalupian (Permian) siliceous deposits from central Guizhou of South China: Regional correlations with implications for carbonate productivity during the Middle Permian biocrisis

Qi Meng [a], Wuqiang Xue [a], Fayao Chen [a], Jiaxin Yan [a,*] jaxy2008@163.com, Jiahua Cai [b], Yadong Sun [a, c], Paul B. Wignall [d], Ke Liu [e], Zhichen Liu [f], Deng Chen [f]

[a] *School of Earth Sciences, State Key Laboratory of Biogeology and Environmental Geology, China University of Geosciences, Wuhan 430074, China*

[b] *Institute for Environmental and Climate Research, Jinan University, Guangzhou 510632, China*

[c] *Humboldt Post-doc Fellow, University of Erlangen-Nuremberg, Schlossgarten 5, 91054 Erlangen, Germany*

[d] *School of Earth and Environment, University of Leeds, Leeds LS2 9JT, UK*

[e] *Wuhan Surveying-Geotechnical Research Institute Co., LTD. of MCC, Wuhan 430080, China*

[f] *102 Geological Party, Guizhou Bureau of Geology and Mineral Exploration and Development, Zunyi 563099, China*

[*]Corresponding author

Abstract

In comparison with the amount of study undertaken on the end-Permian mass extinction, the preceding Guadalupian mass extinction has received little investigation, even though it marks a significant biotic turnover associated with global environmental changes. During the earlier event,

reef carbonate production shut down and was replaced by siliceous, mud-rich deposits (SRDs) in South China. However, changes in carbonate platform productivity during this epoch remain to be clarified. This paper presents sedimentological and conodont biostratigraphic investigations on the Guadalupian SRDs developed on the Yangtze Carbonate Platform (YCP) in central Guizhou. The findings are viewed in the context of Guadalupian sequence correlation of South China successions, which shows that the integrity of the YCP failed to match the platform tectonic evolution. The platform evolution saw the onset of major intra-platform depressions and the gradual onlap by SRDs along the platform margin. Stratigraphic correlation reveals that the platform experienced three phases of onlap by SRDs during the early Roadian, the late Wordian and the late Capitanian upwards. Platform carbonates re-expanded their extent following the first two phases, but not during the final phase. An evolutionary model is proposed for the Guadalupian carbonate platform, which follows the contemporaneous eustatic sea-level fluctuations. The partial drowning observed within the platform interior and increasing retreat along the platform margin could suggest an insufficient carbonate sediment supply shedding from the platform top during the Guadalupian. The variation in carbonate productivity raises our attention to the change in shallow-water carbonate factories, which is closely related to the fortunes of carbonate-secreting biota and environmental factors impacting the carbonate platform producers during the Guadalupian.

Keywords: Guadalupian, Platform shrink, Biocrisis, Carbonate factories, Conodont stratigraphy

1. Introduction

The Middle to Late Permian is a critical interval that saw major disturbances to environments

45 and biota, exemplified by two mass extinctions, during the Middle Permian and at the end-Permian.
46 Although the losses of the Middle Permian mass extinction used to be included in those of the end-
47 Permian mass extinction, the former are now regarded as a distinct crisis (Jin et al., 1994; Stanley
48 and Yang, 1994; Shi et al., 1999; Clapham et al., 2009; McGhee et al., 2013). The Middle Permian
49 mass extinction is variously known as the Guadalupian extinction, end-Guadalupian extinction,
50 Capitanian extinction, mid-Capitanian extinction, and the pre-Lopingian extinction etc. (Jin et al.,
51 1994; Stanley and Yang, 1994; Shen and Shi, 2002; Bond et al., 2010a; Zhang et al., 2019b). Here
52 we adopt the term "Guadalupian mass extinction".

53 The extinction event affected many groups including brachiopods, rugose corals, fusulinid
54 foraminifers and alatoconchid bivalves (Jin et al., 1994; Isozaki and Aljinović, 2009; Wignall et al.,
55 2009a). Records from the Global Stratotype Section and Point (GSSP) sections (Penglaitan, Tieqiao)
56 of the Guadalupian – Lopingian Boundary (GLB) showed the losses spanned the late Capitanian to
57 the earliest Wuchiapingian interval (Jin et al., 2006; Yin et al., 2007; Shen and Shi, 2009; Huang et
58 al., 2018). In SW China (Guizhou, Yunnan, Sichuan provinces), the extinction has been regarded as
59 the "mid-Capitanian mass extinction", corresponding to a major negative excursion of the $\delta^{13}C_{carb}$
60 value within the *Jinogondolella altudaensis – J. prexuanhanensis* conodont Zone, which severely
61 affected photosynthetic and photosymbiont-bearing taxa: green algae and keriothecal-walled
62 fusulinids (Wignall et al., 2009a; Bond et al., 2010b). A similar pattern is recorded in the coeval
63 western Tethys, Panthalassa and the Boreal Realm (Ota and Isozaki, 2006; Isozaki and Aljinović,
64 2009; Bond et al., 2010a; Wignall et al., 2012; Bond et al., 2015; Zhang et al., 2019b).

65 The timing of the event in South China is debated. For example, most large and
66 morphologically complex species in the fusulinid families Schwagerinidae and Neoschwagerinidae

67 disappeared before the mid-Capitanian, and were replaced by an assemblage of smaller fusulines in
68 the latest Guadalupian which persisted into the Wuchiapingian (Fan et al., 2020; Shen et al., 2020).
69 Assessing global diversity databases suggests the supposed extinction event was a more protracted
70 diversity decrease that spanned the entire early-middle Guadalupian (Clapham et al., 2009; Groves
71 and Wang, 2013). In contrast, major environmental changes in the Capitanian Stage, including the
72 eruption of the Emeishan Large Igneous Province (ELIP) in SW China (Zhou et al., 2002; Wignall
73 et al., 2009a), shallow-marine habitat loss caused by great regression (Hallam and Wignall, 1999;
74 Chen et al., 2009; Arefifard, 2017; Wei et al., 2017), marine anoxia (Isozaki, 1997; Zhang et al.,
75 2015), potentially oceanic acidification (Weidlich, 2002a; Clapham and Payne, 2011) and global
76 climate cooling (Isozaki et al., 2007), may have contributed to a short duration mass extinction. It
77 is clearly desirable to examine the geological evidence for changes throughout the Guadalupian to
78 decipher the pattern and mechanism of the Guadalupian mass extinction.

79 Carbonate platforms provide valuable geological archives that result from the interplay of
80 carbonate production and accumulation, and are intrinsically related to changes in the environmental
81 and biotic conditions (*e.g.*, Kiessling et al., 2003; Godet, 2013; Phelps et al., 2015). Carbonate
82 platforms were widely distributed in tropical-temperate zone during the earliest Guadalupian (Fig.
83 1A) (Kiessling et al., 2003; Pomar and Kendall, 2008; Moore and Wade, 2013). However, during
84 the late Guadalupian, the Permian Chert Event saw chert accumulation greatly expand at the expense
85 of carbonate deposition (Murchey and Jones, 1992; Beauchamp and Baud, 2002). Thus, platform
86 carbonates are overlain by cherts in the Guadalupian Series of western North America (Murchey
87 and Jones, 1992; Beauchamp and Baud, 2002; Matheson and Frank, 2020a), Far East Russia (Ueno
88 et al., 2005) and Transcaucasia (Leven, 1998). The main contributors to Permian carbonate platform

89 formation were foraminifers, calcareous algae, along with microbes and reefbuilders (Kiessling et
90 al., 2003). Studies of shallow-water carbonate platforms show a long-term decline in their area from
91 the late Carboniferous to the Middle Triassic (Kiessling et al., 2000; Kiessling et al., 2003), although
92 their coarse stratigraphic resolution prevents analysis of the Guadalupian biocrisis. On the other
93 hand, reef compilations at stage resolution have revealed a gap in reef evolution across the
94 Guadalupian to Lopingian interval (Weidlich, 2002b). The decline in global reef carbonate
95 production (assessed according to their numbers, dimensions and debris potential) has been
96 calculated as nearly 90% (Flügel and Kiessling, 2002). The succeeding early Lopingian was a period
97 of reef recovery (Huang et al., 2017; Wang et al., 2019). Long-term marine acidification
98 (Beauchamp and Grasby, 2012) or climate cooling (Kani et al., 2018) were suggested as the cause
99 of the decline of carbonate production. However, the process of the reduction in carbonate extent,
100 as well as its implications for the coeval biotic and environmental evolution remains unclear.

101 The Yangtze Carbonate Platform (YCP) in South China is one of the tropical platforms that
102 developed during the Guadalupian. It occurred in a relatively simple and well defined tectonic
103 context, although the ELIP erupted in the region towards the end of the Guadalupian. The YCP is
104 well preserved and includes surrounding marginal and basinal facies. In contrast with marine
105 sections elsewhere, where Guadalupian sequences record a major hiatus (*e.g.*, Wignall et al., 2012),
106 South China preserves a relatively complete Guadalupian succession that includes the GSSP of the
107 GLB (Jin et al., 2006). Extensive investigations of fossil records in the Guadalupian strata have
108 provided a high resolution biostratigraphic framework allowing cross-platform correlation.

109 The main objective of this paper is to evaluate the Guadalupian evolution of the YCP in the
110 context of contemporaneous biotic and environmental evolution. We begin with sedimentological

description and conodont stratigraphy of the Guadalupian siliceous deposits from the central part of Guizhou Province, that developed in intra-platform depressions on the YCP. We then construct correlation transects from platforms to basins, to investigate the fluctuations of the carbonate platform extent during the Guadalupian. Finally, a model for the evolution of the YCP is proposed using a sequence stratigraphic framework.

2. Geological setting in South China

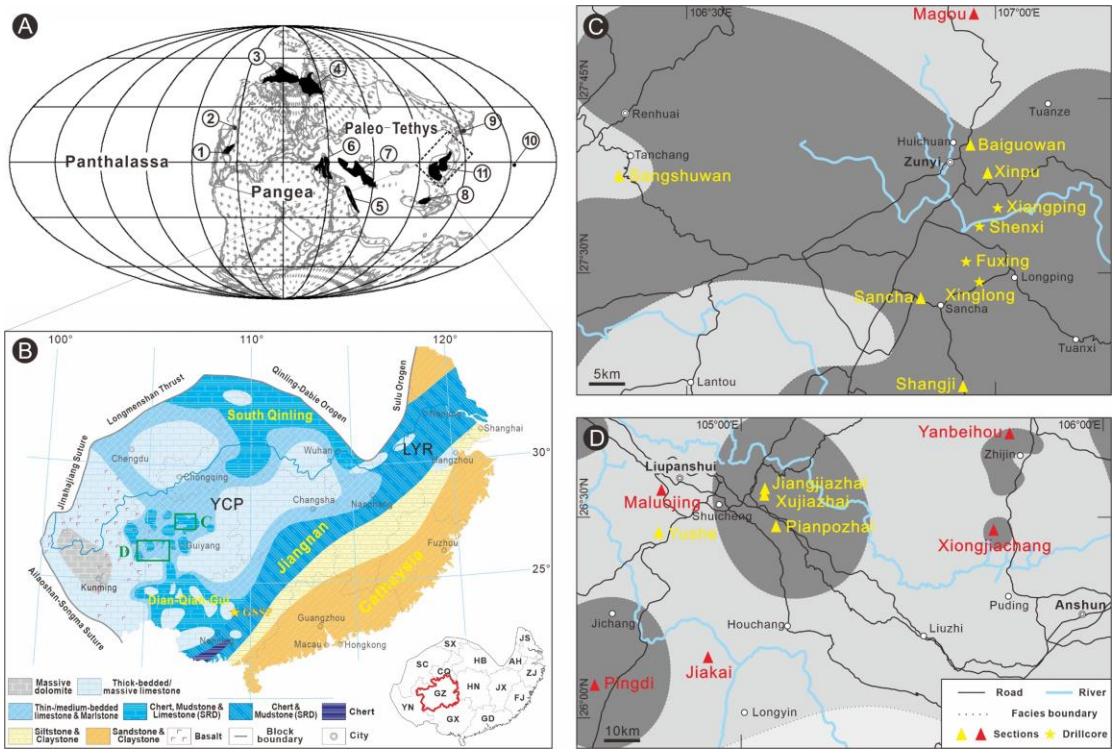

Fig. 1. (A) Middle Permian palaeogeographic map of the world (modified after Kiessling et al., 2003). Locations of Guadalupian carbonate platforms are shown in black. 1 - Delaware Basin; 2 - Phosphoria Sea; 3 - Sverdrup Basin; 4 - Barents Sea; 5 - Arabian platform; 6 - Transcaucasia; 7 - Cimmeria; 8 - Pha Nok Khao platform; 9 - Far East Russia; 10 - Akasaka paleo-atoll; 11 - YCP (this study). (B) Palaeogeographic map of South China during the Middle-Late Guadalupian (modified after Liu and Xu, 1994; Ma et al., 2009; Chen et al., 2018). The two green squares show

the studied Zunyi area (C) and Liupanshui – Anshun area (D) from central Guizhou. Provinces: AH - Anhui; CQ - Chongqing; FJ - Fujian; GD - Guangdong; GX - Guangxi; GZ - Guizhou; HB - Hubei; HN - Hunan; JS - Jiangsu; JX - Jiangxi; SC - Sichuan; SX - Shaanxi; YN - Yunnan; ZJ - Zhejiang. Note that the South China block has rotated ~80° clockwise since the Middle Permian. (C, D) Locality maps of study sections and drillcores. The Magou, Maluojing, Jiakai, Yanbeihou sections are the research sites of Regional Geological Survey Report (1971). The Pingdi and Xiongjiachang sections are the research sites of Sun et al. (2010).

The South China craton is bounded by the Ailaoshan – Songma suture zone, the Jinshajiang suture, the Longmenshan Thrust and the Qinling – Dabie – Sulu orogen, from the southwest and northwest to the north respectively (Fig. 1B) (Wan, 2012; Metcalfe, 2013; Cawood et al., 2018). During the Permian, the plate was situated in the equatorial eastern paleo-Tethys with the Panthalassa Ocean to its east (Fig. 1A) (Kiessling et al., 2003; Scotese, 2014). It comprised the northwest Yangtze Block and the southeast Cathaysia Block, amalgamated along the Jiangnan suture during the Early Paleozoic (Fig. 1B) (Wang et al., 2010; Cawood et al., 2018).

In the Yangtze Block, the Guadalupian succession is dominated by marine carbonate rocks. The main domain of carbonate sedimentation is termed the YCP. It was surrounded by the South Qinling carbonate basin to the north, the Jiangnan chert basin to the east and the Dian – Qian – Gui carbonate basin to the south (Fig. 1B) (Liu and Xu, 1994; Ma et al., 2009). Within these basins, small, isolated carbonate platforms (ICPs) developed with dimensions of tens (occasionally more than one hundred) of kilometres. In the Cathaysia Block, the Guadalupian succession is mainly composed of clastic rocks (Fig. 1B). The clastic material, shedding from the Cathaysia oldland,

147 accumulated in the Jiangnan Basin until the end Guadalupian (Fig. 1B) (Liu and Xu, 1994; Feng et

148 al., 1996).

149

Regions / Series	Western and Southern South China		Northern South China	Eastern South China						
				Lower Yangtze Region			Cathaysian Region			
				Anhui, Jiangsu	Anhui	Zhejiang	Jiangxi	Hunan	Jiangxi	Fujian
Lop.	Xuanwei Wuchiaping Heshan Lungtan	Linghao	Wuchiaping Wangpo shale	Lungtan	Lungtan	Lungtan	Leping	Lungtan(U)	Leping(U)	Cuipingshan
Guadalupian	(Emeishan Basalt)	Linghao	(Wuxue)	Wuxue Yanqiao Yinping		Lengwu	Nangang	Lungtan(L)	Leping(L)	Tongziyan
	Maokou(U)		Kuhfeng	Kuhfeng	Maokou			Dangchong	Chetou	Wenbishan
		Sidazhai(U)	Maokou			Dingjiashan	Maokou			Mingshan
			Chihsia(U)	Chihsia(U)	Chihsia(U)	Chihsia(U)	Chihsia(U)		Xiaojiangbian	Chihsia(U)
Cis.	Maokou(L)	Sidazhai(L)	Chihsia(L)	Chihsia(L)	Chihsia(L)	Chihsia(L)	Chihsia(L)	Chihsia	Chihsia	Chihsia(L)

150

151 Fig. 2. Summary of lithostratigraphic units of the Guadalupian Series from different regions of

152 South China. Units are arranged in chronological order, but not to actual scale. “Lungtan”,

153 “Chihsia”, “Dingjiashan” and “Tongziyan” are also spelled as “Longtan”, “Qixia”, “Tingchiashan”

154 and “Tungtseyan” respectively. Abbreviations: Cis. - Cisuralian; Lop. - Lopingian; L - Lower part

155 of the unit; U - Upper part of the unit.

156

157 The Permian System is divided into three series, the Cisuralian, Guadalupian and Lopingian in

158 ascending order. In South China, the Guadalupian Series is represented by the Maokou Formation

159 and its equivalents in the YCP and ICPs (Fig. 2) (Shen et al., 2018). In the western YCP, the Maokou

160 Formation commonly consists of dolomite and is interbedded with Emeishan basalts in the upper

161 part (Figs. 1B, 2). In the middle-eastern part of the YCP, the Maokou Formation is dominated by

162 bioclastic limestone (Fig. 1B). Outwards from the platform, limestone grades into siliceous

163 limestone and marlstone of the Maokou Formation, or into siliceous, mud-rich deposits (SRDs) of

164 the Kuhfeng Formation in northern South China, and the Sidazhai and Linghao formations in

165 southern South China (the deep-water areas around the ICPs) (Figs. 1B, 2). The SRDs are dominated
166 by thin-bedded chert, sometimes with interbeds of (siliceous) limestone, and/or mudstone, and/or
167 shale.

168 In the Lower Yangtze region (LYR) and the Cathaysian region of eastern South China, the
169 Guadalupian lithostratigraphic units are commonly named provincially (Fig. 2). In terms of
170 lithology, these units comprise carbonate strata of the Maokou, Wuxue, Lengwu, Chihsia (also as
171 "Qixia", upper part) and Xiaojiangbian formations, and SRDs of the Kuhfeng, Nangang, Dangchong,
172 Chetou and Mingshan formations, and clastic strata of the Yanqiao, Yinping, Dingjiashan (also as
173 "Tingchiashan"), Wenbishan, Tongziyan (also as "Tungtseyan"), Lungtan (also as "Longtan", lower
174 part) and Leping (lower part) formations (Fig. 2). It should be noted that the carbonate Chihsia
175 Formation, and the clastic Lungtan and Leping formations are diachronous, and straddle the
176 Cisuralian – Guadalupian and Guadalupian – Lopingian boundaries respectively (see section 5.3).

177 Beneath the Guadalupian succession in South China, the upper Cisuralian Series is composed
178 mainly of the carbonate Chihsia Formation, as well as parts of the Sidazhai and Maokou formations
179 (Fig. 2). The Chihsian limestone is characterised by great thickness and persistence of lithofacies
180 throughout South China. This contrasts with the variation among lithofacies (platform vs. basin)
181 seen in the Maokou Formation during the Guadalupian.

182 The lower part of the Lopingian Series, the Xuanwei, Wuchiaping, Heshan, Lungtan, Leping
183 and Cuipingshan formations, overlie the Guadalupian Series in South China (Fig. 2) (Hou et al.,
184 2020). A shale unit containing coal and volcaniclastic materials, termed the Wangpo Shale, is
185 developed at the base of the Wuchiaping Formation (Fig. 2). An unconformity is widely distributed
186 on the top of the Guadalupian succession of the YCP and interpreted to record uplift related to the

ELIP and/or a Guadalupian regression (He et al., 2003; Sun et al., 2010). However, the time range and duration of this hiatus remain to be determined in most parts of the platform. Carbonate deposition still occurred in South China during the Wuchiapingian, but exhibited considerable differences to Guadalupian time (Liu and Yan, 2009; Yan et al., 2019).

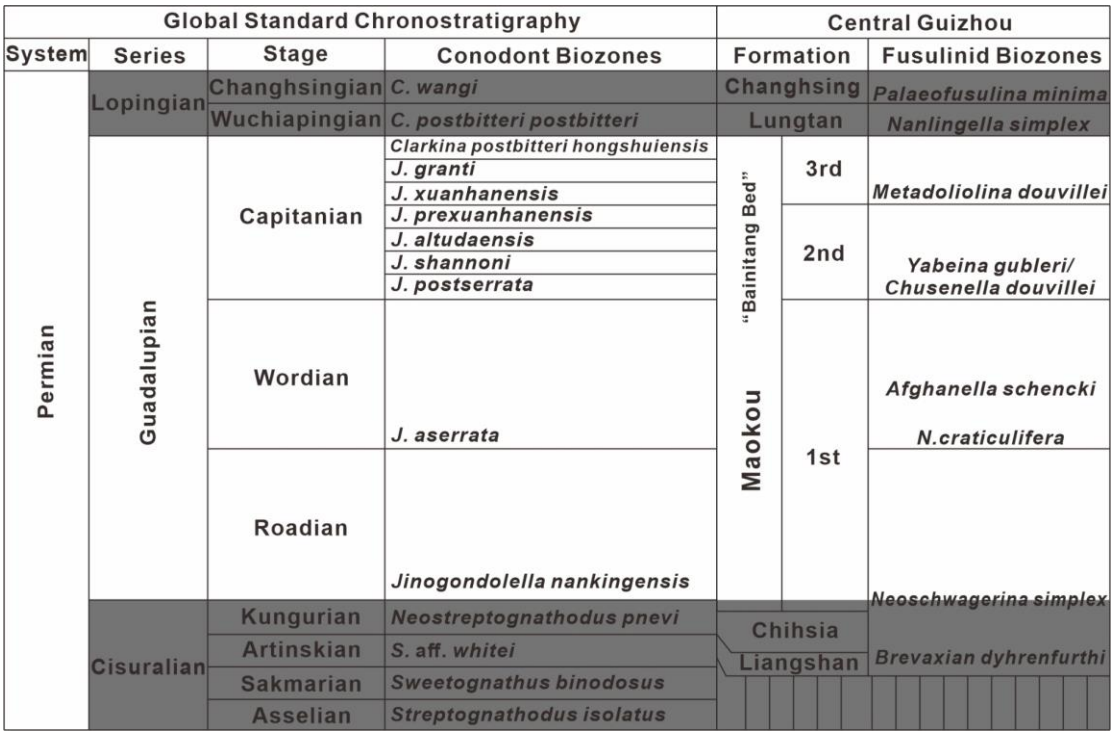

Fig. 3. Subdivision of the Permian sequence of the central part of Guizhou Province and its correlation with the global standard Permian System (combined with works in this research and in Chen et al., 1984; Bureau of Geology and Mineral Resources of Guizhou Province, 1987; Jin et al., 1997; Henderson, 2016; Shen et al., 2018). Conodont biozones and fusulinid biozones of the Cisuralian Series and Lopingian Series are only shown by their First Appearance Datum of species.

The global standard for the Guadalupian biostratigraphy was traditionally based on fusulinid

biozones, but more recently a much higher resolution conodont zonation has been devised. Three stages of the Guadalupian Series, namely Roadian, Wordian and Capitanian, are defined by the nine species within the genus *Jinogondolella* lineage and *Clarkina* lineage (Fig. 3) (Henderson, 2016). In South China, the marine Guadalupian succession is highly fossiliferous, temporally well-constrained by its fossil content (*e.g.*, fusulinid, brachiopod, coral and ammonoid). Stage and series assignment in sections and correlations across the entire region have been mostly achieved by fusulinids and macrofossils (Sheng and Jin, 1994; Shen et al., 2018). However, many sections have conodont biostratigraphic constraints and provide useful reference sections (*e.g.*, Wang, 1995a; Henderson and Mei, 2003; Zhang et al., 2007; Cheng et al., 2017; Sun et al., 2017).

3. Materials and methods

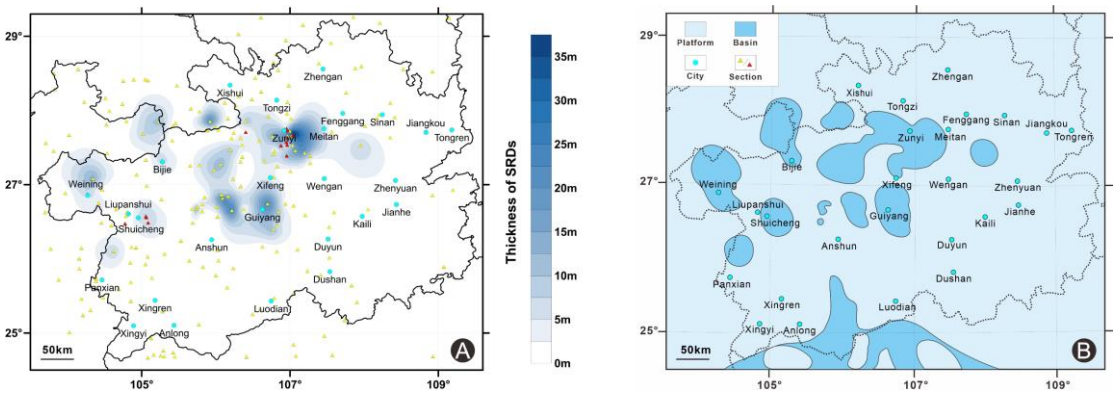

Fig. 4. Middle Permian palaeogeographic map of Guizhou Province. (A) Locations of the collected sections containing Maokou Formation and thickness contour lines of the thin-bedded SRDs. (B) Interpretation of Middle Permian lithofacies in Guizhou. The basin in the southern part of the map is after Liu and Xu (1994) and Ma et al. (2009).

To depict the spatial distribution of the Guadalupian SRDs, a Guadalupian lithofacies map of

Guizhou was compiled (Fig. 4). Stratal sections for the map are collected from the related geological survey sheets covering the region, combined with those undertaken in this study and others observed by the senior authors. Total thickness of the thin-bedded Guadalupian SRDs from the collected sections (data in Appendix A) were plotted on the palaeogeographic map, then contoured with the gridding method by the Surfer 13 software, to constrain the boundaries between the SRDs and the adjacent carbonate deposits (Fig. 4A). The lithofacies map was based on the contour line analysis, along with facies interpretations and biostratigraphic constraints detailed below.

In the Zunyi and Liupanshui – Anshun areas, the Maokou Formation and the lower part of the Lungtan Formation were seen in nine outcrops (Sangshuwan, Baiguowan, Xinpu, Sancha, Shangji, Yushe, Jiangjiazhai, Xujiazhai, Pianpozhai) and four underground drillcores (Xiangping, Shenxi, Fuxing, Xinglong), and were logged and sampled for microfacies analysis and conodont biostratigraphy (Fig. 1C, D).

A total of 272 samples were thin-sectioned for microfacies analysis. Additionally, 38 samples were collected from the limestone beds below, above or within the SRDs for conodont biostratigraphic study in the Pianpozhai, Sangshuwan, Baiguowan, Sancha and Shangji sections. Conodont samples, weighing >5 kg each, were collected from every bed. They were broken into fragments, dissolved using 10% diluted acetic acid, wet sieved through 20 # and 160 # meshes and air-dried. The heavy fraction of insoluble residues was separated using heavy liquid (solution of lithiumheteropolytungstates in water). Conodont specimens were handpicked under binocular microscopes. A total of 405 P1 elements were obtained and seven species were recognised in the genus *Jinogondolella* (Figs. 5, 6).

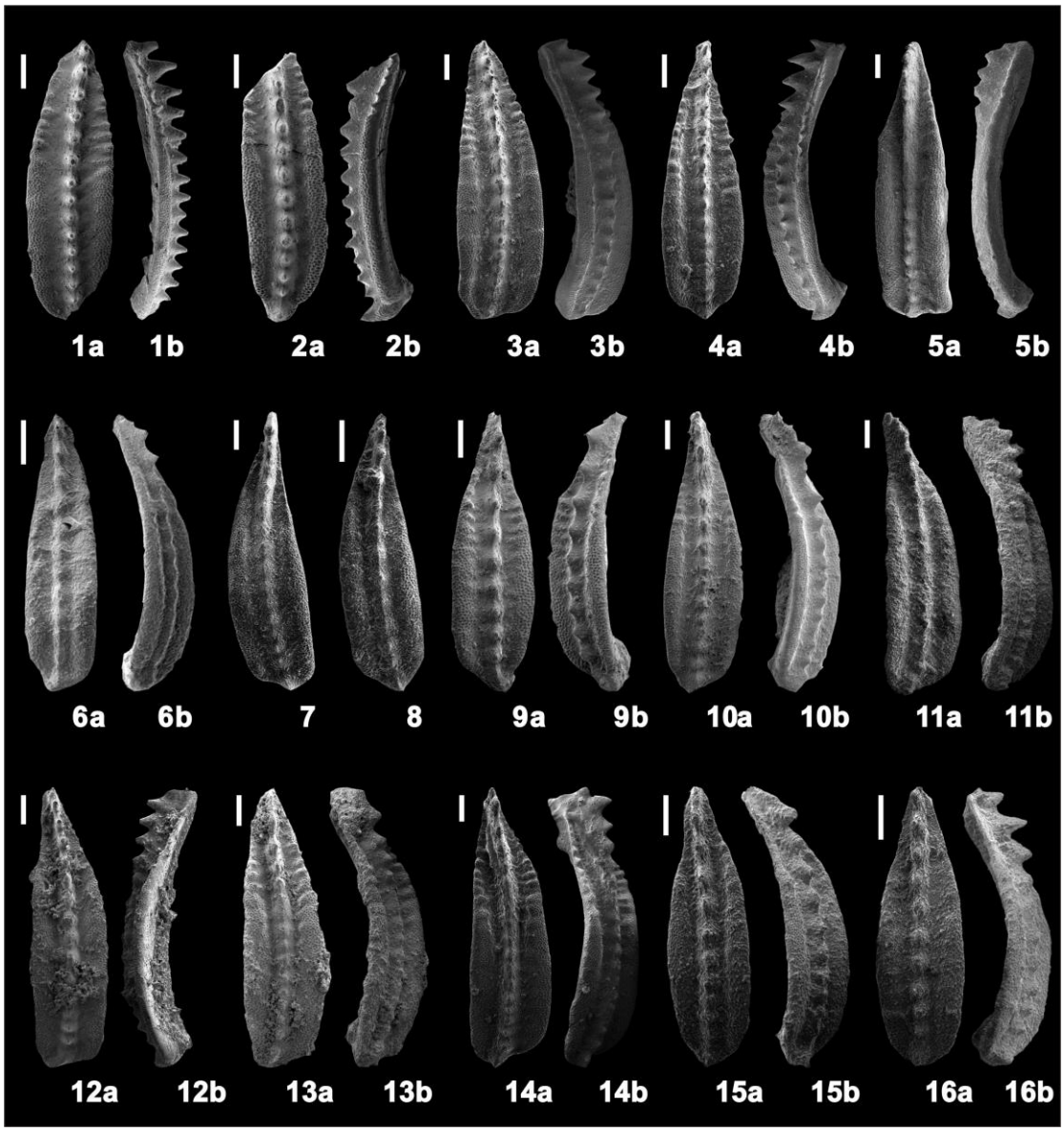

Fig. 5. P1 elements obtained from central Guizhou, scale bar for 100μm, “a” for upper view, “b” for lateral view. 1-2 from Pianpozhai, 3-4 from Shangji, 5-10 from Sancha, 11-16 from Baiguowan. 1, 2, 5: *J. nankingensis* (Wardlaw, 1998), 1. PPZ1, i001001; 2. PPZ1, i001003; 5. SC2, i003028. 3, 9-14: *J. postserrata* (Behnken, 1975), 3. SJ1, i002002; 9. SC3, i003014; 10. SC3, i003015; 11. BGW1, i004134; 12. BGW3, i004106; 13. BGW6, i004056; 14. BGW7, i004014. 4, 15-16: *J. shannoni* (Wardlaw, 1998), 4. SJ1, i002014; 15. BGW1, i004139; 16. BGW2, i004004. 6-8: *J. aserrata* (Clark and Behnken, 1979), 6. SC1, i003024; 7. SC2, i003030; 8. SC2, i003019.

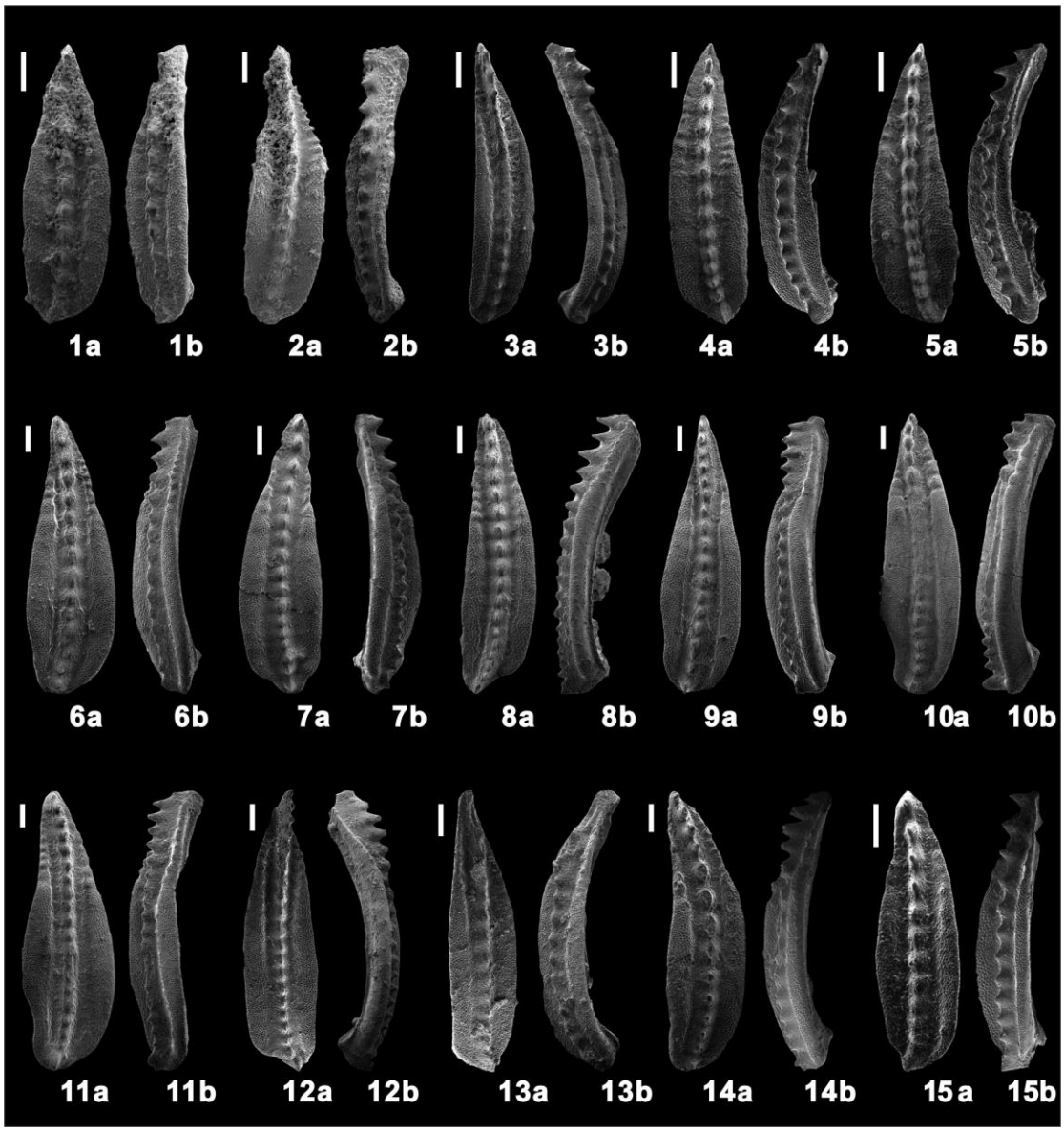

Fig. 6. P1 elements obtained from central Guizhou, scale bar for 100μm, “a” for upper view, “b” for lateral view. 1-11 from Baiguowan, 12-15 from Sangshuwan. 1-3, 13-15: *J. shannoni* (Wardlaw, 1998), 1. BGW3, i004102; 2. BGW6, i004052; 3. BGW7, i004037; 13. SSW1, i006036; 14. SSW2, i006029; 15. SSW3, i006012. 4-7: *J. altudaensis* (Kozur, 1992), 4. BGW8, i005009; 5. BGW9, i005017; 6. BGW10, i005052; 7. BGW11, i005027. 8, 9: *J. prexuanhanensis* (Mei and Wardlaw, 1994), 8. BGW10, i005056; 9. BGW11, i005032. 10, 11: *J. xuanhanensis* (Mei and Wardlaw, 1994), 10. BGW10, i005062; 11. BGW11, i005039. 12: *J. postserrata* (Behnken, 1975), 12. SSW1, i006035.

4. Guadalupian stratigraphy and facies changes in central Guizhou

Combined faunal and lithological features allowed the carbonate strata of the Maokou Formation in Guizhou Province to have been traditionally divided into three members (Fig. 3) (Bureau of Geology and Mineral Resources of Guizhou Province, 1987). However, macrofossils and fusulinid biozone schemes are difficult to apply in central Guizhou, *e.g.*, in the vicinity of Zunyi City (Fig. 1C), where the upper part of the Guadalupian succession above the thick-bedded carbonate rocks of the first Maokouan member consists of thin- to medium-bedded limestone with chert nodules, marlstone, SRDs and manganese deposits. The SRDs in the Zunyi area were assigned to the second Maokouan member by lithology and locally termed the "Bainitang Bed" (Fig. 3) (He and He, 1953). The third Maokouan member was ambiguously thought of either being absent or a manganese (carbonate) deposit (Bureau of Geology and Mineral Resources of Guizhou Province, 1987; Liu et al., 1989). It is still to be determined how many strata from the top of the Maokou Formation have been eroded in this area. A similar situation to the Zunyi area also occurs in the area extending to Liupanshui – Anshun (Fig. 1D). These areas have unique late Guadalupian successions where the "intra-platform trough of central Guizhou" developed (Chen et al., 1984). To understand the stratigraphy and deposition of those Guadalupian successions of the "trough", the Zunyi and Liupanshui – Anshun areas have been studied in detail.

4.1 *Zunyi area*

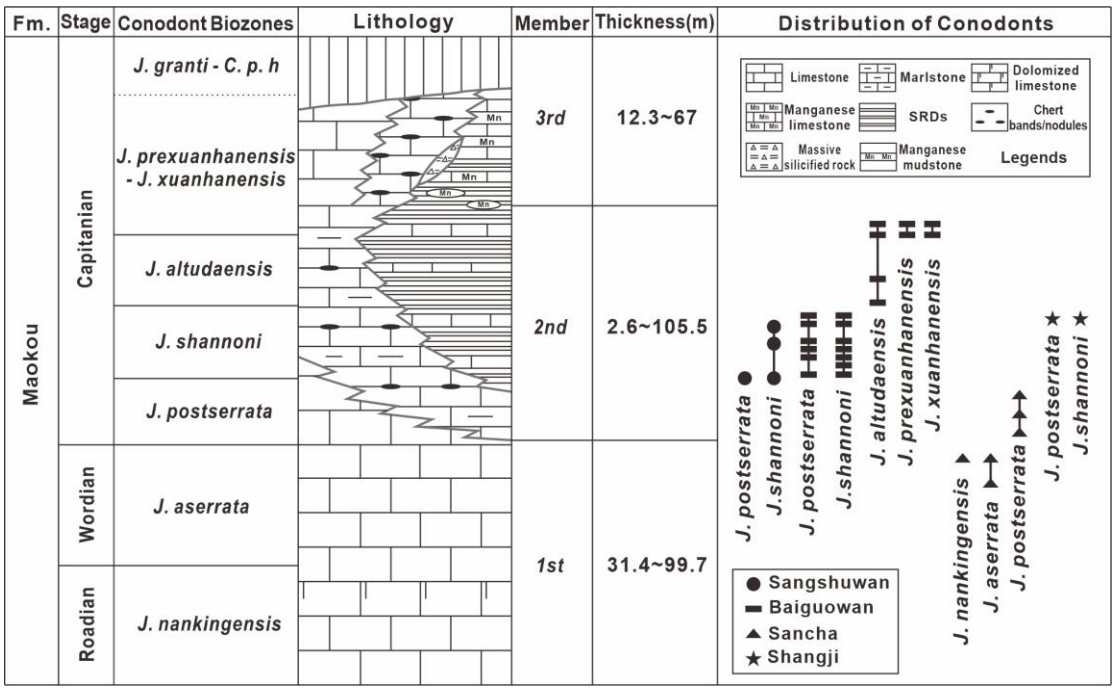

Fig. 7. Composite column of the Maokou Formation in the Zunyi area showing the lithology, thickness and conodont ranges.

The first member of the Maokou Formation is characterised by thick-bedded to massive wacke-packstone of pale grey colour, which is partly dolomitized in the lower part (Figs. 7, 8F, G). It comprises over 40% skeletal grains dominated by foraminifers (including fusulinids), calcareous algae and alatoconchid bivalves (Fig. 8A, B, J-L). Skeletal grains of brachiopods, sponges, gastropods and corals are also common (Fig. 8C-E). At Sancha, *J. nankingensis* (Fig. 5.5) and *J. aserrata* (Fig. 5.6-5.8) specimens were obtained from two samples from the top part of this member, suggesting a Wordian age (Figs. 1C, 7).

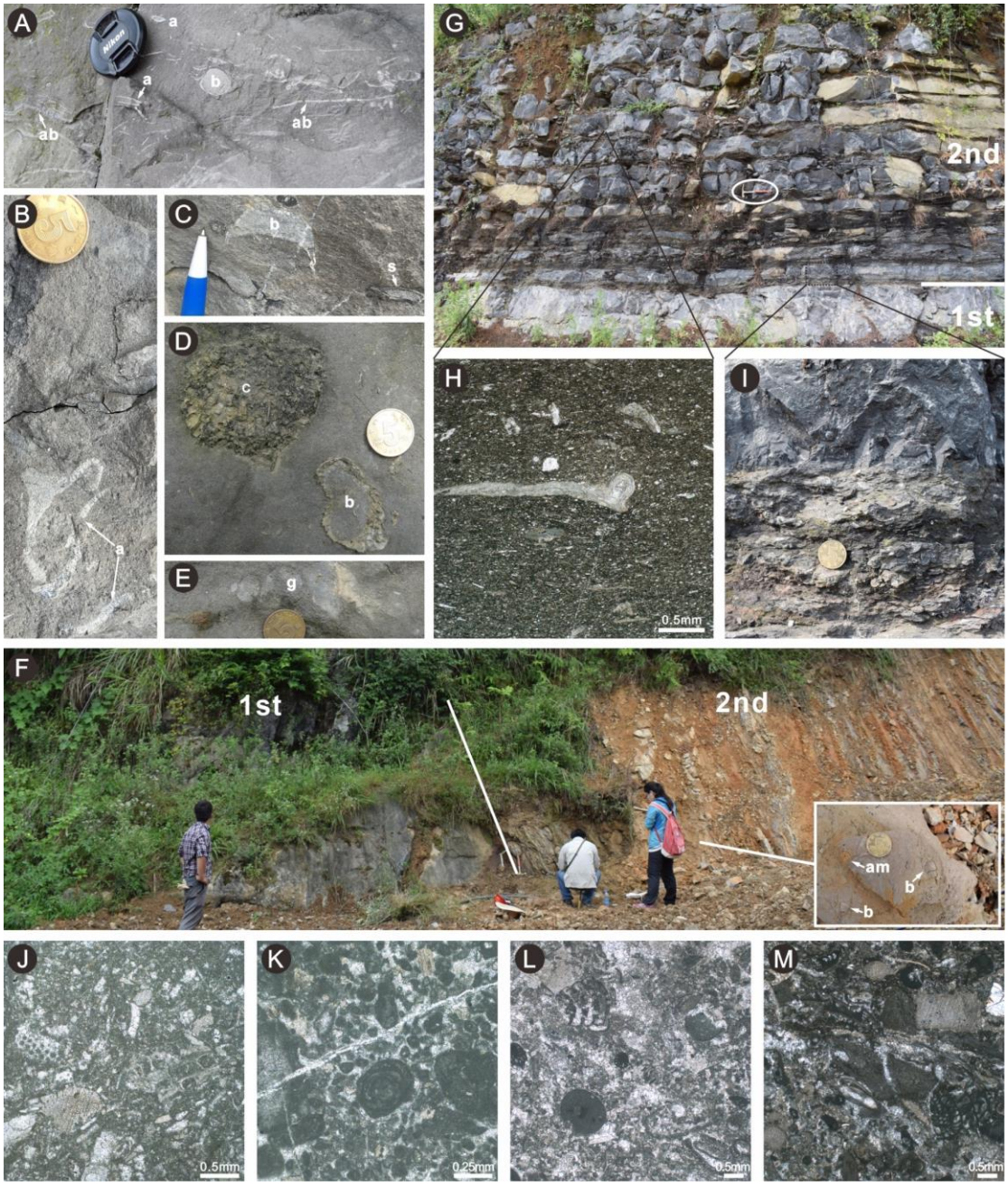

Fig. 8. Sedimentary features of the Maokou Formation in central Guizhou. (A-C) Packstone of the first member at Sangshuwan. (D, E) Packstone of the first member at Sancha. (F) Outcrop photos of the Sancha section. The close-up shows brachiopods and ammonoids found in the SRDs. (G) Outcrop photo of the Baiguowan section. (H, I) Photomicrograph and close-up of wackestone containing brachiopods at Baiguowan. (J) Packstone of the first member containing green algae, foraminifers, crinoids and bryozoans at Baiguowan. (K) Packstone of the first member containing

297 peloids, foraminifers and crinoids at Sancha. (L) Packstone of the first member containing green
298 algae, foraminifers, fusulinids and crinoids at Shangji. (M) Packstone of the first member
299 containing fusulinids, foraminifers, calcareous algae, crinoids and brachiopods at Pianpozhai. The
300 coin is 2 cm in diameter. Abbreviations: a - calcareous algae; ab - alatoconchid bivalves; am -
301 ammonoids; b - brachiopods; c - corals; g - gastropods; s - sponges.
302
303 In the second member, thin-bedded marlstone and SRDs are common (Fig. 7). In the outlying
304 area, the second member is represented by medium-bedded limestone with intercalations of marl
305 and chert bands (Figs. 7, 8G, 9A, C). The medium-bedded wacke-packstone contains 15% – 70%
306 of skeletal grains dominated by brachiopods and also includes foraminifers, crinoids and ostracods
307 (Fig. 8H, I). Eastwards from Sangshuwan and southwards from Magou, marl and chert bands
308 gradually decrease and SRDs become dominant (Figs. 1C, 4). Because of the exploration of
309 carbonate manganese deposits in the Zunyi area, lots of drillcores are available through the
310 Guadalupian succession. The drillcores and outcrops show that the SRDs are dark grey to black in
311 colour and are occasionally interbedded with thin-bedded wackestone or siliceous limestone (Fig.
312 9D, E). The thickness of the SRDs reaches the maximum at Xiangping (Figs. 1C, 4A). The SRDs
313 have only 5% – 10% of fine skeletal grains including sponge spicules, radiolarians, ostracods,
314 ammonoids and brachiopods (Figs. 8F, 9G-J).
315 In the lower part of the second member, *J. postserrata* is present at Sancha (Fig. 5.9, 5.10), and
316 assemblages consisting of *J. postserrata* (Figs. 5.11-5.14, 6.12) and *J. shannoni* (Figs. 5.15, 5.16,
317 6.1-6.3, 6.13-6.15) are recovered at Baiguowan and Sangshuwan. In limestone interbeds of the
318 SRDs, an assemblage with *J. postserrata* (Fig. 5.3) and *J. shannoni* (Fig. 5.4) occurs at Shangji, and

319 *J. altudaensis* (Fig. 6.4, 6.5) at Baiguowan. These conodont fossils indicate that the second member

320 ranges from the early to middle Capitanian age (Fig. 7).

321

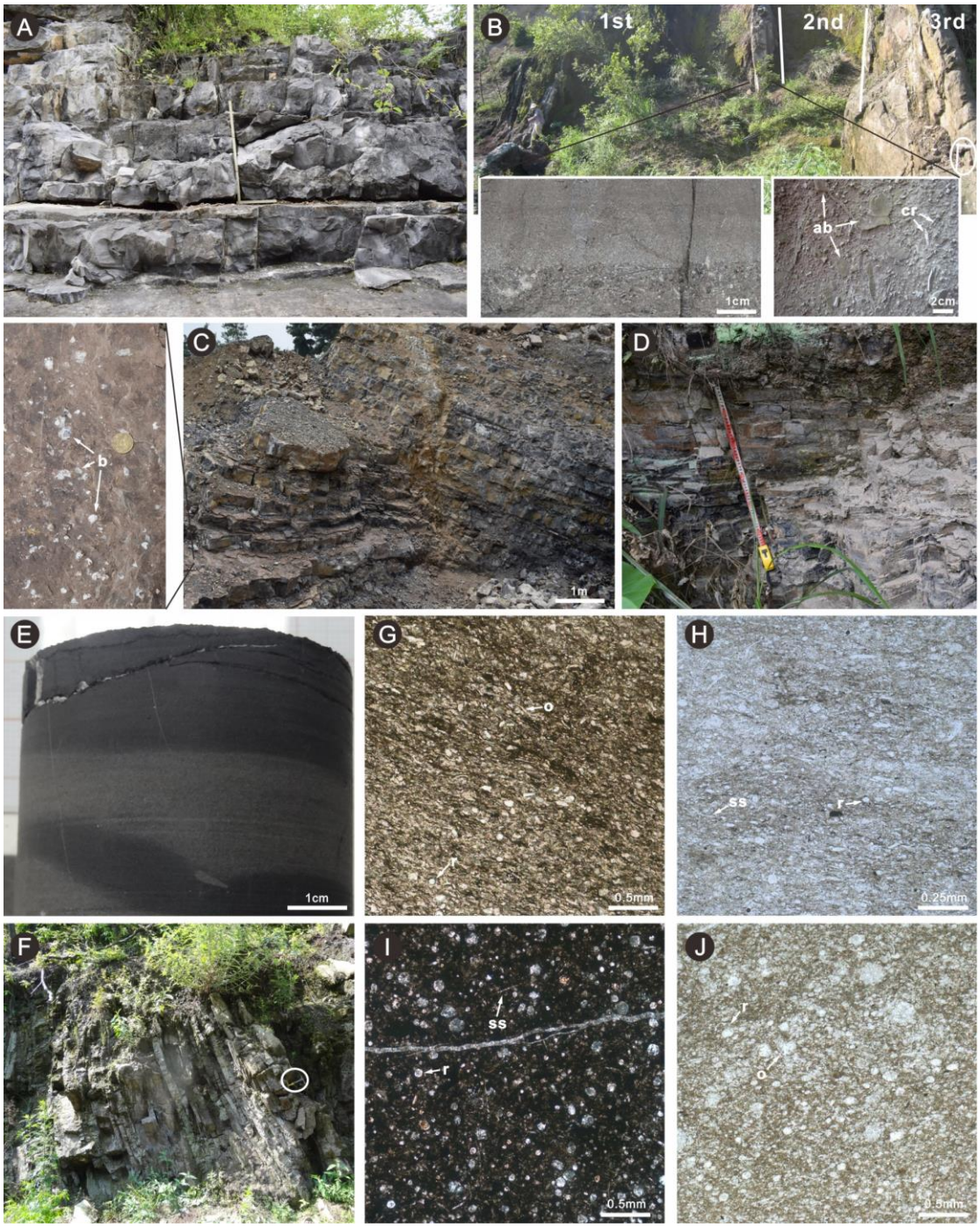

322

323 Fig. 9. Sedimentary features of the Maokou Formation in central Guizhou. (A) Wackestone

324 interbedded with thin-bedded limestone and chert bands of the second member at Sangshuwan.

(B) Outcrop photos of the Pianpozhai section. The close-ups show packstone of the uppermost part of the first member containing alatoconchid bivalves and crinoids. (C) Wackestone interbedded with thin-bedded marlstone of the second member at Baiguowan. The close-up shows brachiopod fossils. (D-F) SRDs of the second member at Shangji (D), Shenxi (E) and Jiangjiazhai (F). (G-J) Photomicrographs of SRDs of the second member containing radiolarians, sponge spicules and ostracods at Baiguowan (G), Sancha (H), Xiangping (I) and Shangji (J). The coin is 2 cm in diameter. Each section of the folding ruler is 20 cm in length. Abbreviations: ab - alatoconchid bivalves; b - brachiopods; cr - crinoids; o - ostracods; r - radiolarians; ss - sponge spicules.

The development of the third member in the Zunyi area is indicated by conodonts of late Capitanian age. At Baiguowan, limestone interbeds of the uppermost SRDs yielded an assemblage consisting of *J. altudaensis* (Fig. 6.6, 6.7), *J. prexuanhanensis* (Fig. 6.8, 6.9) and *J. xuanhanensis* (Figs. 6.10, 6.11). Thus, a stratal record of the upper Capitanian Stage in the Zunyi area has been confirmed, at least as high as the *J. prexuanhanensis – J. xuanhanensis* Zone (Fig. 7).

The palaeogeography of the late Capitanian is generally similar to that of the early-middle Capitanian. In the siliceous deposition area (*e.g.*, in the Shangji section and the four drillcores), there occur manganese mudstone or manganese carbonates, intercalated with siliceous deposits (Figs. 7, 10J). Laterally, medium-bedded micrite and wackestone with chert nodules occur, and these deposits gradually transition into thick-bedded packstone, *e.g.*, at Magou and Sancha (Fig. 10I). Skeletal grains in packstone comprise mainly crinoids, foraminifers (including fusulinids), brachiopods, and minor ostracods and bryozoans (Fig. 10H).

347 At certain locations, an interval of approximately 10-m-thick massive silicified rocks is
348 observed. This interval has informally been referred to as “city-wall chert” in the literature for its
349 brecciated and weathering-resistant appearance (Regional Geological Survey Report, 1971). At
350 Sangshuwan, there are many siliceous clasts supported by silicified matrix in the lower part of these
351 massive rocks (Fig. 10C, D). The clasts are platy or cubic in shape, with diameters ranging from 3
352 to 35 cm. Most clasts exhibit dark grey banding (Fig. 10C). The orientations of the clasts, judging
353 by their lengths or interior bands, range from chaotic to roughly parallel to the original bedding
354 upwards (Fig. 10C). The upper part of the interval exhibits continuous beds of thin-bedded, banding
355 silicified deposits (Fig. 10A, B) to massive, nodular sediments. At Baiguowan, the interval is
356 massive (Fig. 10E). The clasts in the rocks are angular and range from 0.5 to 30 cm in diameter,
357 whilst no banding is identified in these clasts (Fig. 10E). At both locations, skeletal grains in
358 silicified clasts, including crinoids, foraminifers (including fusulinids) and calcareous algae, are
359 observed (Fig. 10F, G).
360 The Guadalupian Maokou Formation in the Zunyi area is unconformably overlain by plant-
361 bearing clay, siltstone or coal layers of the Lungtan Formation (Fig. 10I, K).
362

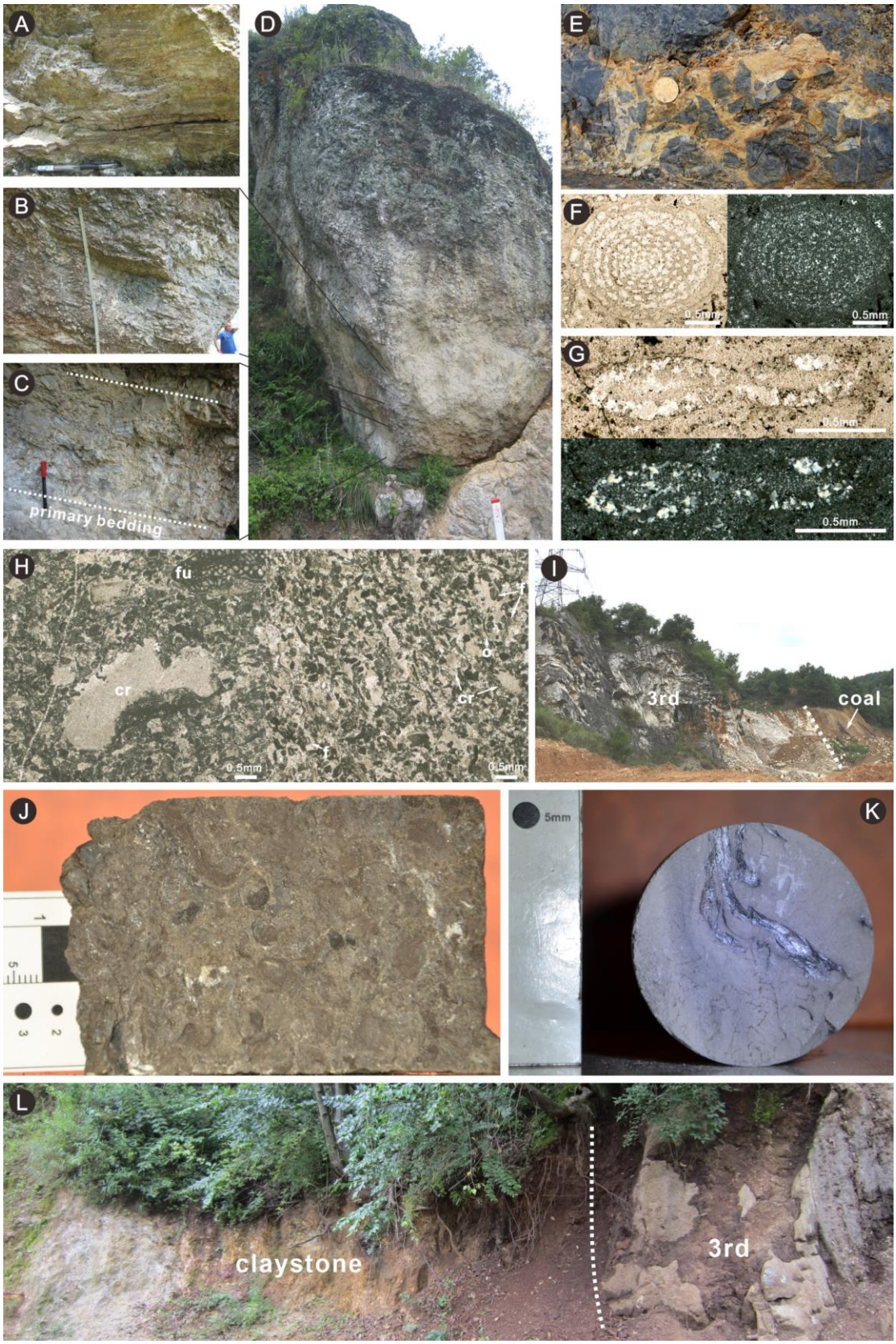

363

364 Fig. 10. Sedimentary features of the Maokou Formation in central Guizhou. (A-C) Close-ups show

365 massive silicified rocks of the third member at Sangshuwan. Note the primary bedding and clasts

with dark grey bands in C. (D) Outcrop photo of massive silicified rocks of the third member at Sangshuwan. A is found behind D and could be traced to the upper part of D. (E) Outcrop photo of massive silicified rocks of the third member at Baiguowan. (F, G) Photomicrographs of silicified fusulinid (F), green algae (G) and matrix in the massive silicified rocks at Baiguowan. They are under the plane and perpendicular polarized light respectively in the same horizon. (H) Photomicrographs of packstone of the third member at Sancha. (I) Outcrop photo of the Sancha section. (J) Manganese carbonate of the third member at Shenxi. (K) Claystone of the Lungtan Formation at Shenxi. (L) Outcrop photo of the Xujiazhai section. Each section of the folding ruler is 20 cm in length. Abbreviations: cr - crinoids; f - foraminifers; fu - fusulinids; o - ostracods.

4.2 *Liupanshui – Anshun area*

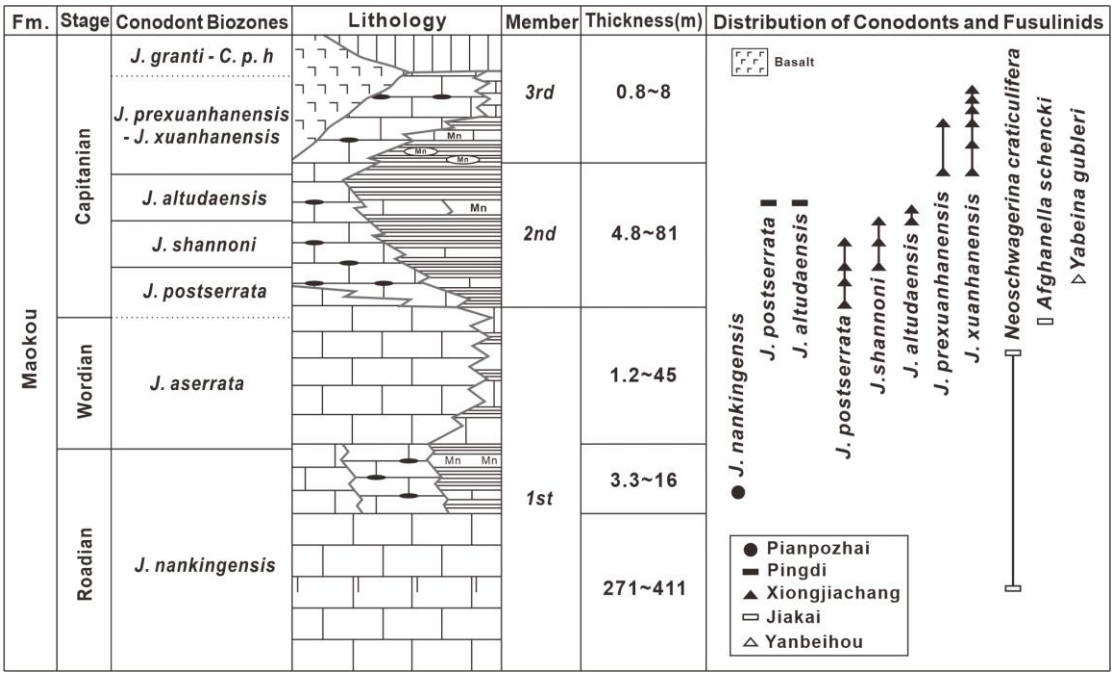

Fig. 11. Composite column of the Maokou Formation in the Liupanshui – Anshun area showing the lithology, thickness, conodont and fusulinid ranges. See Fig. 7 for legends.

381

382 The first member of the Maokou Formation is mainly characterised by grey, thick-bedded to
383 massive packstone, with a bed of dolomitized limestone in the lower part (Fig. 11). The packstone
384 comprises ~70% skeletal grains including foraminifers (including fusulinids), calcareous algae,
385 crinoids and brachiopods (Fig. 8M). Fusulinids *Neoschwagerina craticulifera* (Schwager, 1883) and
386 *Afghanella schencki* (Thompson, 1946) collected from this member at Jiakai indicate a Roadian-
387 Wordian age (Fig. 11) (Regional Geological Survey Report, 1971). However, in the middle or upper
388 part of the first member, thin- to medium-bedded wackestone alternates with SRDs and manganese
389 mudstone at Jiangjiazhai, Xujiazhai and Pianpozhai (Fig. 1D), and upwards the limestone beds
390 become thicker packstone with fragmented shells of alatoconchid bivalves and crinoids (Figs. 9B,
391 11) (Chen et al., 2018). Laterally, the wackestone is interbedded with chert bands at Yushe,
392 Maluojing and Yanbeihou (Figs. 1D, 11). Skeletal grains comprise only ~15% of the wackestone
393 and include brachiopods, foraminifers, ostracods, whilst 10% of the SRDs consist of sponge spicules.
394 *Jinogondolella nankingensis* specimens (Fig. 5.1, 5.2) are identified from the thin-bedded
395 wackestone at Pianpozhai. Thus, these siliceous beds in the first member accumulated during the
396 Roadian (Fig. 11).

397 In the second member, thin-bedded SRDs occur at Jiangjiazhai, Xujiazhai, Pianpozhai, Pingdi
398 and Xiongjiachang, and they are occasionally interbedded with manganese mudstone (Figs. 1D, 9F,
399 11). The SRDs have ~10% skeletal grains including sponge spicules, ostracods, radiolarians and
400 foraminifers. Laterally, the second member passes from SRDs to medium- to thick-bedded
401 wackestone with chert bands (Fig. 11). According to the conodont biostratigraphic investigation of
402 Sun et al. (2010) at Xiongjiachang and Pingdi, this member of SRDs and wackestone is of early-

403 middle Capitanian age (Fig. 11).

404 The third member is characterised by alternations of medium- to thick-bedded micrite with
405 chert nodules and packstone (Figs. 10L, 11). The packstone comprises ~55% crinoids, foraminifers
406 (including fusulinids) and brachiopods. The carbonates are commonly covered by basalt in the
407 Liupanshui – Anshun area whilst in the Xujiazhai and Yanbeihou sections, the carbonates are
408 overlain by the claystone of the Lungtan Formation (Fig. 10L). At Xiongjiachang, Sun et al. (2010)
409 identified the *J. prexuanhanensis – J. xuanhanensis* Zone of the late Capitanian in this member,
410 implying that the late Guadalupian erosion has removed less than two conodont zonations of strata,
411 not as much as almost the entire Capitanian suggested by He et al. (2003).

412

413 4.3 *Facies interpretations and changes in central Guizhou*

414 Based on field observations and microfacies analysis, three facies types have been recognised
415 in the Maokou Formation from central Guizhou.

416 *Type 1*: Light grey, thick-bedded wacke-packstone with abundant skeletal grains or peloids.
417 Skeletal grains consist of foraminifers (including fusulinids), calcareous algae, brachiopods,
418 crinoids and alatoconchid bivalves, suggesting deposition in warm, sunlit waters of shallow
419 platform environments (Schlager, 2003; Flügel, 2010).

420 *Type 2*: Grey, thin- to medium-bedded wacke-packstone sometimes alternating with marl or
421 siliceous beds. Skeletal grains are lower in diversity than *Type 1* facies and are dominated by
422 brachiopods and gastropods. Other grains, such as foraminifers, ostracods and crinoids are only
423 present occasionally. This assemblage indicates that this facies type develops in a somewhat deeper
424 platform environment as evidenced by the absence of calcareous algae.

425 *Type 3*: Dark grey to black SRDs composed mainly of thin-bedded siliceous and argillaceous
426 strata, and occasionally interbedded with thin-bedded limestone or lenticular, manganese mudstone.
427 Skeletal grains are dominated by sponge spicules and radiolarians. Brachiopods, ammonoids,
428 ostracods and foraminifers occur occasionally, and are smaller than the fossils seen in facies *Type*
429 *2*. The fossil assemblage suggests a deep-water basinal setting. The total thickness contour lines of
430 SRDs in this type indicate that the faices are scattered on the platform (Fig. 4), rather than forming
431 a linear trough or a series of rifts in the region (Chen et al., 1984; Luo et al., 1988). Thus, this facies
432 is interpreted to have formed in intra-platform depressions in central Guizhou.

433 Based on the facies interpretations and the biostratigraphy above mentioned, the spatial-
434 temporal change in depositional facies has been constrained. During the early Roadian, central
435 Guizhou was a shallow-water carbonate platform across the region. By the late Roadian, deeper-
436 water facies commenced in the Liupanshui – Anshun area (*e.g.*, *Type 2* at Xujiazhai, Yushe,
437 Maluojing and Yanbeihou; *Type 3* at Jiangjiazhai and Pianpozhai), whilst shallow platform facies
438 persisted elsewhere (Fig. 11). Later during the Wordian, the basinal deposits at Jiangjiazhai and
439 Pianpozhai alternated with packstone containing abundant fragmented alatoconchid bivalves, and
440 deeper platform deposits at the other locations turned to shallow platform wacke-packstone (*Type*
441 *1*) with well-preserved fusulinid shells (Fig. 11).

442 During the early Capitanian, deeper platform and local basinal facies recurred in the
443 Liupanshui – Anshun area and initiated in the Zunyi area (Figs. 7, 11). In the *J. prexuanhanensis* –
444 *J. xuanhanensis* Zone of the late Capitanian, limestone with chert nodules or manganese carbonates
445 commonly filled depressions in both the Zunyi and Liupanshui – Anshun areas (Figs. 7, 11).

446 The depositional interpretation of the massive silicified rocks during the late Capitanian

447 requires further investigation. These rocks only occur in specific sections in the Zunyi area and
448 differ from the SRDs of facies *Type* 3, *e.g.*, these massive silicified rocks contain shallow-water
449 organisms and low organic matter and argillaceous contents. All of the clasts and the corresponding
450 matrix were silicified, so these rocks appear massive. In addition, the silicified rocks differ from
451 place to place in regard to the clast types, sizes, shapes and depositional successions. Xu et al. (2020)
452 recently measured the silicon isotopes and REE values of these massive silicified rocks and
453 suggested that the observed brecciation and silicification resulted from hydrothermal migration
454 along potential syndepositional faults during the stage of the ELIP.
455
456 **5. Guadalupian sequence stratigraphy around the YCP**
457
458 In order to evaluate the spatial-temporal relationship between the Guadalupian carbonate rocks
459 and the SRDs, and the origin of deep-water deposits in central Guizhou, we have investigated the
460 Guadalupian successions around the YCP. The lithostratigraphic units from different regions are
461 summarized in Fig. 2 and detailed information on sections is in Appendix B.
462

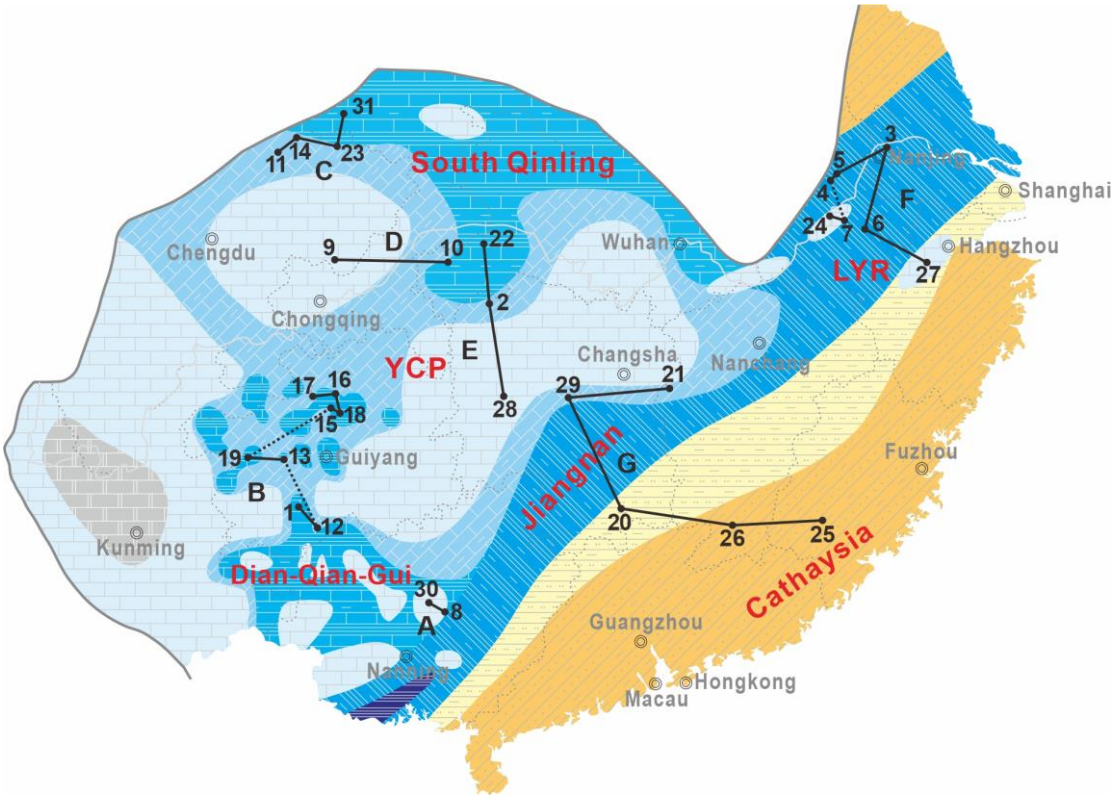

Fig. 12. Index map showing localities of transects for correlations of the Guadalupian sequence stratigraphy in South China.

5.1 *Southern South China*

In the southern region of South China, the YCP passes into the Dian – Qian – Gui Basin (Fig. 1B). SRDs interfinger with shallow-water carbonates on the margins of the YCP as well as the ICPs found within the basin. Transect A is along depositional dip and intersects the Laibin – Heshan ICP (Fig. 12). Transect B involves a correlation from the exterior to the interior of the southern part of the YCP (Fig. 12).

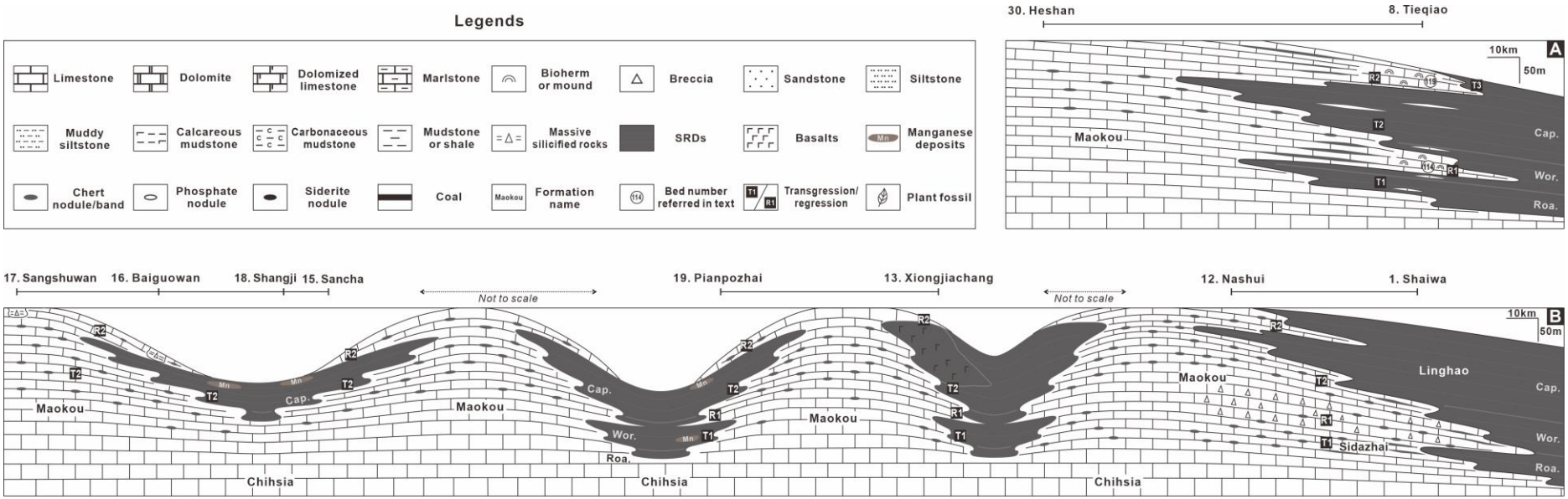

Fig. 13. Correlation of the Guadalupian sequence stratigraphy in the southern region of South China (transects A, B). See Fig. 12 for localities of transects and Appendix B for detailed information on sections. Conodont biostratigraphic version follows that in Fig. 3. Abbreviations: Roa. - Roadian; Wor. - Wordian; Cap. - Capitanian.

Transect A

The Tieqiao section in the transect is a supplementary reference section of the GSSP for the GLB. Intensive biostratigraphic investigations on this section make its Guadalupian Series a key reference for intra- and inter-regional correlation (Sha et al., 1990; Mei et al., 1999; Wang and Sugiyama, 2001; Jin et al., 2006). The basal part of the Guadalupian succession consists of medium-bedded bioclastic limestone, yielding *J. nankingensis* of Roadian age. The main body of the succession comprises SRDs with two massive carbonate intervals (Bed 114 and 119 of Sha et al., 1990) (Fig. 13A). The latter two intervals are mound-shaped bodies, individually ranging from a few metres to tens of metres in thickness, and from tens of metres to over one hundred metres in extent (Chen et al., 2009; Yao et al., 2012). The carbonates include sponge-*Tubiphytes* bafflestone and bryozoan-*Tubiphytes* framestone, as well as packstone, grainstone and floatstone containing crinoids, bryozoans, calcareous algae and alatoconchid bivalves (Chen et al., 2009; Yao et al., 2012; Huang et al., 2018). Laterally, the mound flanks become thin-bedded SRDs and limestone. Bed 114 spans within the *J. aserrata* Zone of Wordian age (Sun et al., 2017), whilst Bed 119 spans the *J. xuanhanensis* Zone to the *C. postbitteri hongshuiensis* Zone of late Capitanian age (Sun et al., 2017). The transition northwest from Tieqiao into the interior of the Laibin – Heshan ICP is a transition into bioclastic limestone (Fig. 13A). Here, a late Guadalupian erosion surface is draped by a thin bauxite layer between the Maokou and the overlying Heshan formations (Yu et al., 2016).

Transect B

Transect B encompasses the “trough” located in the southern margin of the YCP where the Guadalupian succession comprises the Sidazhai and the overlying Linghao (or Shaiwa) formations

500 in the Shaiwa section, and the main part of the Maokou Formation in the shallower Nashui section
501 (Fig. 13B).

502 The Sidazhai Formation at Shaiwa consists mainly of thin- to medium-bedded micrite, with
503 sparse clasts showing graded bedding (Wang et al., 2016). Starting in the Roadian Stage, thin-
504 bedded SRDs also occur alternating with the micrite beds, and from the late Roadian to early
505 Wordian, thick-bedded breccia beds are present (Fig. 13B) (Wang et al., 2016). The succeeding
506 Linghao Formation, characterised by SRDs, started in the early Capitanian *J. postserrata* Zone
507 (Wang et al., 2016).

508 In the Nashui section, the Guadalupian succession begins with Roadian strata: thick-bedded
509 bioclastic limestone and is overlain by medium-bedded limestone with chert nodules (Fig. 13B) (Shi
510 et al., 2000; Henderson and Mei, 2003). These are succeeded by massive coarse carbonate
511 megabreccias, containing abundant fusulinids and calcareous algae, that span the late Roadian to
512 the Wordian (Shi et al., 2000; Henderson and Mei, 2003). This interval correlates with the breccia
513 beds found in the Shaiwa section (Fig. 13B). Starting at the late Wordian, the megabreccias were
514 overlain by thin-bedded siliceous limestone and SRDs in ascending order (Shi et al., 2000).
515 Subsequently, limestone with chert nodules reappeared in the late Capitanian *J. prexuanhanensis* –
516 *J. xuanhanensis* Zone (Fig. 13B) (Henderson and Mei, 2003). The limestone beds are
517 unconformably covered by strata of the Wuchiaping Formation.

518

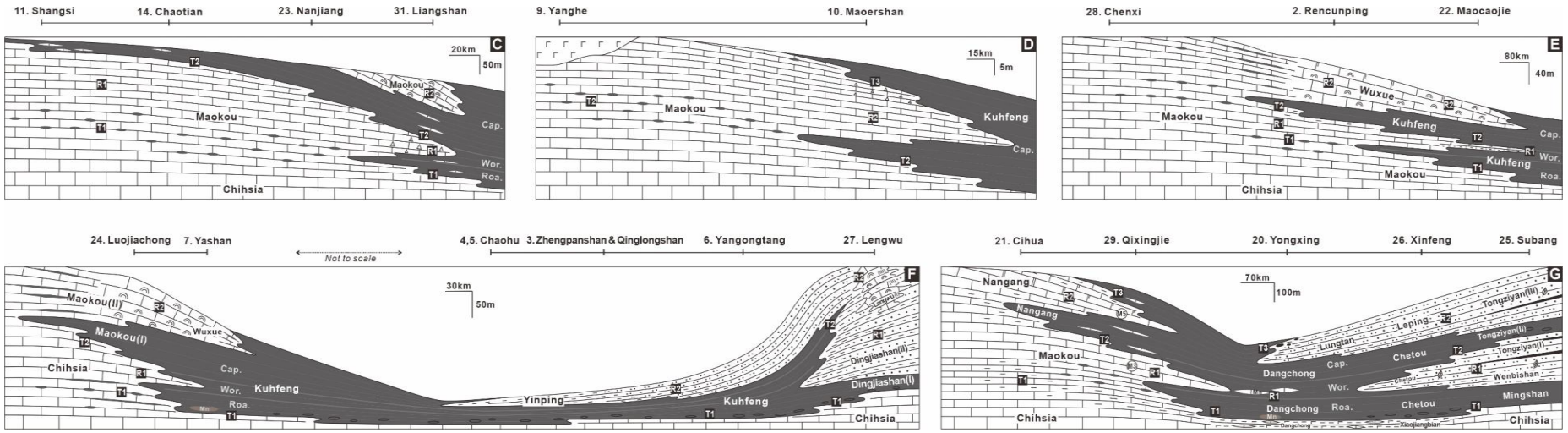

519

520 Fig. 14. Correlation of the Guadalupian sequence stratigraphy in the northern (transects C, D, E) and eastern (transects F, G) regions of South China. See Fig. 12 for

521 localities of transects, Fig. 13 for legends and Appendix B for detailed information on sections. Conodont biostratigraphic version follows that in Fig. 3.

522 Abbreviations: Roa. - Roadian; Wor. - Wordian; Cap. - Capitanian.

523

524 5.2 *Northern South China*

525 In the northern part of South China, the YCP passes northwards into the South Qinling Basin
526 and an embayment developed in western Hubei (Fig. 1B). The bay formed during the early
527 Guadalupian (Liu and Xu, 1994; Ma et al., 2009). Three transects (C, D, E) from basin to platform
528 facies are correlated here (Fig. 12).

529

530 *Transect C*

531 This transect includes the Liangshan, Nanjiang, Chaotian and Shangsi sections (Fig. 14C). At
532 Liangshan, the Guadalupian succession includes the uppermost part of the Chihsia Formation and
533 the Maokou Formation (Kong, 2011). Three carbonate intervals are separated by two SRD intervals
534 (Fig. 14C). The lower and the upper carbonate intervals are thick-bedded and massive bioclastic
535 limestone respectively (Fig. 14C). Fossils in the former interval are dominated by crinoids and
536 brachiopods, and in the latter by calcareous algae, crinoids and sponges (Kong, 2011; Cao et al.,
537 2018). The middle carbonate interval is breccia consisting of micrite intraclasts. The lower
538 limestone yielded the conodont *J. nankingensis* of the Roadian (Wang, 1978).

539 The Nanjiang, Chaotian and Shangsi platform sections are similar: the Maokou Formation
540 consists of a lower limestone member and an overlying SRD member (Fig. 14C). The former is
541 mainly packstone rich in calcareous algae and brachiopods, with chert nodules present in the lower
542 part (Fig. 14C) (Lai et al., 2008). The limestone member continues to the early Capitanian *J.*
543 *postserrata* Zone (Mei et al., 1994; Sun et al., 2008). The layers with chert nodules are dated to the
544 lower *J. aserrata* Zone of the early Wordian (Sun et al., 2008). The SRD member contains
545 intercalated limestone beds that increase upwards and also southwestwards from Chaotian to

546 Shangsi (Lai et al., 2008). However, the youngest conodont zone recorded in the upper SRD
547 members varies: it is the *J. altudaensis* Zone at Nanjiang, the *J. shannoni* Zone at Chaotian and the
548 upper *J. postserrata* Zone at Shangsi respectively (Mei et al., 1994; Sun et al., 2008). The top contact
549 thus gets gradually older towards the platform interior (Fig. 14C).

550 The upper massive bioclastic limestone noted from the Liangshan section is obviously a
551 distinct limestone horizon in the transect for it occurs above the SRDs (Fig. 14C).

552

553 *Transects D and E*

554 Transects D and E both trend from the basinal embayment in western Hubei to the northern
555 part of the YCP (Fig. 12). The Maoershan section in transect D, as well as the Maocaojie and
556 Rencunping sections in transect E, record a deeper-water environment, with the Rencunping section
557 being closer to the platform (Fig. 12).

558 In transect D, the Capitanian Stage of the Maoershan section (Tianfengping of Wei et al., 2016)
559 includes two intervals of limestone and two intervals of SRDs (Fig. 14D). The lower limestone is a
560 bioclastic grainstone, with *J. altudaensis* yielded from the topmost horizons and the overlying SRDs
561 also developed in the *J. altudaensis* Zone of the middle Capitanian (Zhang et al., 2007). The upper
562 limestone is composed of packstone and breccia upwards. Conodont *J. granti* obtained in the top
563 part of the breccia bed indicates a late Capitanian age for the following SRDs (Zhang et al., 2007).

564 In transect E, the Guadalupian succession includes, in ascending order, the Maokou, Kuhfeng
565 and Wuxue formations. The Maokou Formation is a thick-bedded bioclastic limestone containing
566 brachiopods, corals and fusulinids (Fig. 14E) (Tian et al., 2007; Cao et al., 2018). In the middle part
567 of the Maokou Formation at Rencunping, there occurs an interval with abundant chert nodules (Fig.

14E) (Cao et al., 2018). The Kuhfeng Formation is mainly SRDs and contains ammonoids, sponge spicules and radiolarians (Shi et al., 2016; Cao et al., 2018). In the Maocaojie section, an interval of carbonaceous mudstone with dolomitized limestone interbeds occurs in the middle part of the SRDs (Fig. 14E) (Tian et al., 2007; Shi et al., 2016). Overlying the Kuhfeng Formation is the thick-bedded to massive limestone of the Wuxue Formation that contains abundant carbonate mud and calcareous algae and fusulinids, and is partly dolomitized in the upper part (Fig. 14E) (Tian et al., 2007; Cao et al., 2018).

According to the biostratigraphic data from the Maocaojie section and the nearby Luojiaba section, the Maokou Formation underlying the Kuhfeng SRDs remains within the Roadian Stage (Fig. 14E), supported by fossils of the *J. nankingensis* conodont Zone and *Pseudoalbaillella globosa* radiolarian Zone (Ma et al., 2016; Shi et al., 2016). In the Kuhfeng SRDs, the intercalated dolomitized limestone and carbonaceous mudstone are constrained to the *Follicucullus monacanthus* radiolarian Zone of the Wordian Stage (Shi et al., 2016). Upwards, the Kuhfeng SRDs continue into the middle Capitanian *F. scholasticus* radiolarian Zone, suggesting a late Capitanian age of the Wuxue Formation in the top part of the Maocaojie section (Fig. 14E) (Shi et al., 2016).

In the carbonate-dominated Rencunping section, the Maokouan limestone exhibits a longer range than that at Maocaojie and spans from the Roadian to the early Capitanian *J. postserrata* Zone (Fig. 14E) (Cao et al., 2018). Horizons bearing chert nodules in the middle part of the limestone yielded *J. aserrata* of the Wordian (Cao et al., 2018), coeval with those nodules in the Shangsi section from transect C (Fig. 14C, E). Specimens of *J. prexuanhanensis* identified in the uppermost part of the Kuhfeng Formation and *J. xuanhanensis* identified in the Wuxue Formation indicate that the *J. prexuanhanensis – J. xuanhanensis* Zone is the highest Capitanian biozone in the area (Cao

et al., 2018).

The interior YCP successions in the Yanghe and Chenxi sections are mainly bioclastic limestone (Fig. 14D, E) (Mu et al., 1997; Liu et al., 2016a). In the Yanghe section, chert nodules are observed in the upper part of the Maokou Formation within the middle Capitanian *J. altudaensis* Zone. The Maokou Formation there is overlain by Emeishan basalts (Fig. 14D) (Liu et al., 2016a). The Guadalupian successions in both sections are truncated at an unconformity surface.

5.3 *Eastern South China*

During the Guadalupian, there were three depositional regimes in the eastern part of South China, the carbonate deposits of the YCP's margin and the ICPs in the west, the siliceous deposits of the Jiangnan Basin in the middle, and the terrestrial clastic deposits of the Cathaysian region in the east (Fig. 1B). Transects F and G stretch across the three regimes allowing lateral correlations of the carbonate, siliceous and terrigenous depositional systems to be seen (Fig. 12).

Transect F

Transect F is mainly in the LYR where the Chaohu, Zhengpanshan, Qinglongshan, Yangongtang and Lengwu sections array along a depositional trend approaching and intersecting with the Cathaysian region (Figs. 12, 14F). The Guadalupian biostratigraphy of the LYR has been intensively studied. The Chaohu, Zhengpanshan and Yangongtang sections are basinal locations that yield abundant deep-water fossils such as radiolarians, ammonoids and conodonts. The Zhengpanshan section is the locality where the holotype of the conodont species *J. nankingensis* was found (Jin, 1960). The standard radiolarian biozones of the Middle Permian, as well as the

612 widely recognised Kuhfeng Formation, have been established in this area (Wang and Qi, 1995).

613 The Guadalupian successions of the Chaohu, Zhengpanshan, Qinglongshan and Yangongtang
614 sections are composed of thick-bedded limestone in the basal part, thin-bedded SRDs in the lower
615 part, and thin- to thick-bedded clastic deposits in the upper part (Fig. 14F). The Chihsia Formation
616 in the basal part contains abundant fusulinids, corals and brachiopods (Kametaka et al., 2005). The
617 SRDs of the Kuhfeng Formation are subdivided into a lower mudstone member with phosphate
618 nodules, and an upper chert member yielding radiolarians, sponge spicules and bivalves (Kametaka
619 et al., 2005; Kametaka et al., 2009; Zhang et al., 2019b). The overlying Yinping (or Yanqiao)
620 Formation consists of siltstone at Yangongtang, which passes basinwards (northwestwards) into
621 shale with trace fossils at Zhengpanshan, Qinglongshan and Chaohu (Figs. 12, 14F) (Kametaka et
622 al., 2005; Du et al., 2010; Zhang et al., 2020).

623 At Lengwu, close to the Cathaysia oldland, the Guadalupian succession is composed of the
624 Chihsia (top part), Dingjiashan and Lengwu formations in ascending order (Figs. 2, 14F) (Wang,
625 1993; Liu et al., 2016b). The Chihsia Formation is mainly a thick-bedded bioclastic limestone (Feng,
626 1991). The Dingjiashan Formation comprises a lower member of SRDs with phosphate nodules and
627 fossils of ammonoids and sponge spicules, and an upper member of mudstone-sandstone
628 alternations that yielded ammonoids, brachiopods and foraminifers (Fig. 14F) (Feng, 1991). The
629 carbonate Lengwu Formation consists of massive sponge framestone and bafflestone in the lower
630 and upper members, and medium-bedded crinoid-bearing marlstone with siltstone interbeds in the
631 middle member (Fig. 14F) (Wang, 1993; Liu et al., 2016b).

632 As indicated by conodont biostratigraphy and zircon U-Pb dating, SRDs of the lower part of
633 the Kuhfeng Formation and the lower part of the Dingjiashan Formation are of early Roadian age

(Wang, 1993; Wu et al., 2017; Zhang et al., 2019b). *Jinogondolella aserrata* of the Wordian has been reported from the lower carbonate member of the Lengwu Formation in the Lengwu section (Wang, 1993). These data constrain the mudstone-sandstone alternations of the upper part of the Dingjiashan Formation of the late Roadian, and the marlstone of the middle part of the Lengwu Formation of the early Capitanian (Liu et al., 2016b).

The distribution of siliciclastic deposits in the transect F demonstrates that there was a terrigenous supply derived from the southeastern Cathaysia oldland. From Lengwu to Yangongtang, and to Zhengpanshan and Chaohu, the siliciclastic successions gradually decrease in thickness and grain size as the terrigenous source becomes more distal (Fig. 14F). Consistent with the decrease, the base of siliciclastic deposits becomes younger to the northwest. Terrigenous deposits did not occur at Chaohu until the late Capitanian (Zhang et al., 2019b).

The Yashan and Luojiachong sections were located around the margin of an ICP, and were distant from the Cathaysian terrigenous input (Fig. 12). The Kuhfeng Formation at Yashan is similar to that at Chaohu, Zhengpanshan, Qinglongshan and Yangongtang, but the upper succession is the carbonate Wuxue Formation, pale grey, thick-bedded to massive bafflestone and bindstone built by calcareous algae, *Tubiphytes* and sponges, and wackestone to grainstone with abundant crinoids, calcareous algae and fusulinids (Figs. 2, 14F) (Luo et al., 1997; Du et al., 2010). These carbonates are mound-shaped with their dimensions ranging from tens to about one hundred metres, and laterally they pass rapidly into thin-bedded SRDs (Chen et al., 1995). The fusulinid genus *Metadoliolina* indicates a late Capitanian age for the Wuxue Formation (Luo et al., 1997; Kametaka et al., 2009). Considering the age assignment of the similar carbonate strata from the northern part of the YCP (*e.g.*, Rencunping and Maocaojie sections of Transect E), the Wuxue Formation of the

Yashan section probably belongs to the late Capitanian *J. prexuanhanensis – J. xuanhanensis* Zone.

The Luojiachong section was closer to the platform than the Yashan section. The Guadalupian succession is composed of two carbonate units separated by an SRD unit (Fig. 14F). The lower unit belongs to the upper part of the Chihsia Formation and the upper two units are grouped into the Maokou Formation (Wang, 1993). The upper part of the Chihsia Formation is mainly a dark grey, thick-bedded bioclastic limestone that yielded Roadian to Wordian conodonts of the *J. nankingensis* and *J. aserrata* zones (Wang, 1993). Similar to the Shangsi and Rencunping sections in the northern part of the YCP, horizons rich in chert nodules and chert interbeds are present in the lower part of the thick-bedded limestone (Fig. 14F). The succeeding SRD unit yielded *J. postserrata* of early Capitanian age (Wang, 1993). The upper carbonate unit is a pale grey, massive limestone with calcareous algae, crinoids, fusulinids and sponges (Luo et al., 1997). This unit is roughly dated as the late Capitanian by Chen et al. (1995), so it is correlatable with the above mentioned Wuxue Formation in the LYR and northern part of the YCP.

Transect G

The Subang, Xinfeng and Yongxing sections are a transition from the Cathaysia Block to the Jiangnan Basin, and are mainly the record of terrigenous and siliceous depositional systems (Fig. 12). Further to the northwest, the Qixingjie and Cihua sections progress from the Jiangnan Basin into the carbonates of the YCP (Fig. 12).

In the Subang section, the Guadalupian succession includes, in ascending order, limestone from the top part of the Chihsia Formation, the siliceous Mingshan Formation, and the siliciclastic Wenbishan and Tongziyan formations (Figs. 2, 14G). The Mingshan Formation (equivalent to the

678 widespread Kuhfeng Formation in the LYR) consists of black SRDs (Du and Zhang, 1998; Li, 2008).
679 The overlying Wenbishan Formation is mainly thin-bedded siltstone and silty mudstone with
680 brachiopods, bivalves and ammonoids. The Tongziyan Formation includes three members (Fig.
681 14G). The lower and upper members are medium- to thick-bedded, fine-grained sandstone and
682 siltstone with plant fossils and interbeds of coal. The middle member is mudstone with phosphate
683 nodules (Li, 2008). The brachiopods *Neoplicatifera huangi* (Jin et al., 1974) and *Monticulifera*
684 *sinensis* (Frech, 1911), and the ammonoid *Shouchangoceras shouchangensis* (Zhao and Zheng,
685 1977) present in the Wenbishan and Tongziyan formations indicate a Wordian-Capitanian age (Li,
686 2008). In the Wuping section, about 80 km from Subang, the fusulinid *Metadoliolina* obtained from
687 the limestone interbeds in the upper part of the Tongziyan Formation indicates a late Capitanian age
688 (Li, 2008).

689 In the Xinfeng and Yongxing sections from Jiangxi and Hunan provinces respectively, the
690 Guadalupian successions comprise three lithological units. The first unit is characterised by
691 calcareous mudstone with abundant limestone lenses, the second unit mainly includes SRDs, and
692 the third unit is dominated by siliciclastics (Fig. 14G). Differences in the division scheme and
693 naming of these units occur because geological surveys were conducted independently in these two
694 provinces (Fig. 2). At Xinfeng, the first unit is called the Xiaojiangbian Formation, which is
695 equivalent to the top part of the Chihsia Formation (Figs. 2, 14G) (Zhang, 1997; Liu, 2008). The
696 second unit of SRDs is termed the Chetou Formation and contains phosphate nodules in the basal
697 part and horizons of siltstone-sandstone with plant fossils in the middle part (Fig. 14G) (Liu, 2008).
698 In the Yongxing section, the first two units are assigned to the Dangchong Formation (Figs. 2, 14G).
699 The SRD unit consists of manganese mudstone interbeds in the basal part and an interval of

manganese limestone in the middle part (Fig. 14G) (Wang, 1995b). The Chetou and Dangchong formations are commonly considered synonymous with the Kuhfeng Formation (Liu, 2008). In both sections, the lower part of the Chetou and Dangchong formations yielded ammonite genera (*Altudoceras*, *Waagenoceras* and *Paraceltites*) typical of the Roadian to Wordian interval (Bureau of Geology and Mineral Resources of Jiangxi Province, 1984; Zhang, 1997; Liu, 2008). The regional stratigraphic correlation by Wang (1995b) suggested that the horizons of siltstone-sandstone and the manganese limestone intercalated in the middle parts of the two formations were likely Wordian (Fig. 14G). Thus, the upper parts of these two formations probably belong to the Capitanian.

The third siliciclastic unit is locally termed the Leping Formation at Xinfeng and the Lungtan Formation at Yongxing (Figs. 2, 14G). These successions mainly consist of sandstone and siltstone fining upwards into mudstone and siltstone interbedded with siderite nodules at the latter locality (Fig. 14G) (Wang, 1995b; Liu, 2008). Limestone interbeds in the lower parts of the two formations yielded the fusulinid *Metadoliolina multivoluta* (Sheng, 1963) and ammonoids such as *Paratongluceras* (Zhang, 1997; Liu, 2008). The Leping and Lungtan formations are common Late Permian units in South China. The strata discussed here only belong to the lower part of the succession and contain late Guadalupian fossils.

Dominated by the terrigenous supply originating from the Cathaysia oldland, the distribution of siliciclastics of the Tongziyan, Leping and Lungtan formations in transect G is similar to that in transect F. Both show trends of getting finer and younger towards the west (Fig. 14G) (Zhou, 1985; Liu, 2008).

In the Qixingjie section from Hunan Province, the basal Guadalupian succession is a bioclastic limestone of the Chihsia Formation and the main body of the succession is the Maokou Formation

(Fig. 14G). The lower part of the Maokou Formation mainly comprises thin-bedded marlstone and siliceous limestone (Fig. 14G). The upper part includes two intervals of thick-bedded limestone (Bed M3 and M5 of Wang, 1995b), both of which are overlain by an interval of SRDs (Fig. 14G). Wang (1995b) assigned the basal part of the Maokou Formation to the Roadian and correlated Bed M3 with the manganese limestone horizons of the Wordian, and the dolomized Bed M5 with the sandstone and siltstone of the late Capitanian in the Yongxing section.

The Cihua section from Jiangxi Province was located at the eastern margin of the YCP. Its Guadalupian succession includes medium-bedded limestone of the top part of the Chihsia Formation, and the Maokou and Nangang formations in ascending order (Figs. 2, 14G). The Maokou Formation consists of black, thin-bedded marlstone and micrite yielding bivalves in the lower part, and of dark grey, thick-bedded to massive bioclastic limestone bearing fusulinids in the upper part (Fig. 14G) (Zeng et al., 2010). The Nangang Formation starts with SRDs and passes upwards into medium- to thick-bedded bioclastic limestone and dolomite yielding fusulinids and corals (Fig. 14G) (Zeng et al., 2010).

The occurrence of fusulinid *Neoschwagerina craticulifera* (Schwager, 1883) indicates that the top part of the Chihsia Formation and the Maokou Formation are of Roadian-Wordian age (Zeng et al., 2010). The overlying Nangang Formation started in the early Capitanian and the late Capitanian fusulinid *Metadoliolina* was found in its upper part (Zeng et al., 2010).

5.4 *Guadalupian sequence correlation in South China*

Correlations of the strata successions with the updated biostratigraphic constraints discussed above help establish a sequence stratigraphic framework for the Guadalupian succession of South

744 China. The sequences recorded here mainly reflect transgressive (T) - regressive (R) cycles
745 (Catuneanu et al., 2009), namely T1 to T3, and R1 to R2 respectively. Although some gravity-flow
746 deposits, such as massive breccia developed adjacent to some platform margins, are incorporated in
747 the regressive phase, it is not possible to distinguish lowstand or shelf margin system tracts. During
748 transgressive phases, SRDs of slope and basin facies expanded their extent and during regression
749 shallow-water limestone was better developed.
750
751 *Southern South China*
752 In the Tieqiao reference section, the Maokou Formation is subdivided into three third-order
753 sequences (Mei et al., 1999; Hu et al., 2012; Yao et al., 2012). Transgression T1 is indicated by the
754 transition from the limestone of open platform facies to the SRDs of basin and slope facies during
755 the Roadian (Fig. 13A) (Yao et al., 2012; Sun et al., 2017). Upwards, the two massive carbonate
756 intervals (Bed 114 and 119 of Sha et al., 1990) are interpreted as bioherms based on their mound-
757 like forms, smaller sizes (commonly tens of metres in dimension) and prominent components of
758 sedentary organisms (such as calcareous algae and sponges) (Chen et al., 2009; Yao et al., 2012).
759 Intercalated in siliceous basinal and slope deposits, and featured by phototrophic organisms
760 (calcareous algae and alatoconchid bivalves), the massive mounds accumulated in relative shallow-
761 water environments to the underlying and overlying siliceous deposits, correlating to the R1 and R2
762 regressions respectively (Fig. 13A). Bed 114 is constrained to the Wordian Stage, indicating that
763 R1 belongs to the early Wordian, and the T2 transgression, above the Bed 114, started in the late
764 Wordian (Sun et al., 2017). Wignall et al. (2009b) detailed the succession in the Bed 119 at Tieqiao
765 and identified a transgressive surface within the Capitanian *J. granti* Zone. The thin-bedded

766 limestone above the surface of Bed 119 coupled with the succeeding SRDs indicates the third
767 transgression T3, which persisted into the Wuchiapingian (Fig. 13A). Thus, there were two and a
768 half T-R cycles in the Guadalupian sequence. This scheme from Tieqiao is applicable throughout
769 South China although the sequence boundaries require further study.

770 Guadalupian sequences on the southern slope of the YCP are recorded in the Shaiwa and
771 Nashui sections (Fig. 13B). During the Roadian, the occurrence of chert beds and nodules within
772 the limestone in both sections correlates well with the T1 transgression of Tieqiao (Fig. 13B). Above
773 this, the breccia beds in the two places are traceable, and at Nashui the carbonate lithoclasts
774 (megabreccias) were mainly derived from the shoal margin and had sizes up to tens of centimetres
775 (Meng et al., 2018). The breccia beds are therefore interpreted as the products of R1 regression.

776 Along the slope, the T2 transgression is distinct (Fig. 13B). In the Shaiwa section, this
777 transgression is evidenced by the substitution of the siliceous Linghao Formation for the carbonate-
778 dominated Sidazhai Formation (Wang et al., 2016). In the Nashui section, the transgression is
779 indicated by the decrease of bed thickness, from massive breccia to well-bedded siliceous limestone
780 and SRDs in ascending order. The succeeding limestone with chert nodules represents the R2
781 regression (Fig. 13B) (Mei et al., 1999; Henderson and Mei, 2003).

782 In central Guizhou, the Guadalupian sequence in the intra-platform depressions is also
783 correlatable with that of Tieqiao. Two transgressions, T1 and T2, are developed: the Roadian basinal
784 SRDs in the Liupanshui – Anshun area, and the early Capitanian basinal SRDs and equivalent
785 deeper platform siliceous limestone throughout central Guizhou (Fig. 13B). The intervening R1
786 regression could be represented by the local recovery of platform deposits in the basins of T1 in the
787 Liupanshui – Anshun area (Figs. 11, 13B). Overlying the T2 deposits, the R2 regression could be

788 related to the shallowing seen in the late Capitanian such as transitions from SRDs to manganese
789 carbonate or limestone (Figs. 7, 11, 13B).
790
791 *Northern South China*
792 In northern South China, the Guadalupian T-R cycles recognised in the Tieqiao section are also
793 traceable. The T1 transgression is seen as an onlap of the early Roadian platform carbonates by
794 basinal SRDs in the Liangshan and Maocaojie sections (Fig. 14C, E). Traced towards the interior of
795 the YCP, the T1 is manifest as horizons of deeper platform limestone with chert nodules in the
796 Nanjiang, Chaotian, Shangsi and Rencunping sections (Fig. 14C, E). Subsequently, in basinal areas,
797 the R1 regression is developed as breccia at Liangshan, and as carbonaceous mudstone and
798 dolomitized limestone interbeds at Maocaojie. In the deeper platform area, the R1 is represented by
799 the re-establishment of shallow, platform carbonate facies (Fig. 14C, E).
800 The succeeding T2 transgression of the early-middle Capitanian is widely present and saw the
801 onlap of basinal SRDs onto platform limestone at Nanjiang, Chaotian, Shangsi, Maoershan and
802 Rencunping (Fig. 14C-E). In the intra-platform area at Yanghe, the transgression is manifest as chert
803 nodules within limestone (Fig. 14D). Above the basinal SRDs of the middle Capitanian, both of the
804 massive limestone of bioherm facies at Liangshan, Maocaojie and Rencunping (Cao et al., 2018),
805 and the packstone of shallow platform facies at Maoershan (Zhang et al., 2007) indicate a shallowing
806 during the R2 regression (Fig. 14C-E). This regression resulted in an exposure of the platform and
807 a major truncation of the preceding Capitanian succession in the area. Conodont biostratigraphic
808 work reveals that at least two biozones of the Capitanian Stage are absent around the platform
809 margin (*e.g.*, two absent at Rencunping) and more are absent towards the platform interior (*e.g.*,

four absent at Nanjiang vs. six at Shangsi) (Figs. 3, 14C, D) (Mei et al., 1994; Sun et al., 2008).

The latest Capitanian deep-water SRDs dated by conodont *J. granti* at Maoershan confirm there was a transgression synchronous with the T3 transgression in the area (Fig. 14D) (Zhang et al., 2007).

Eastern South China

In eastern South China, a similar Guadalupian sequence framework is developed in the carbonate and terrigenous settings in the region.

Overlying the Chihsian carbonates, the widespread deposition of basinal SRDs, including the Kuhfeng, Dingjiashan, Dangchong, Chetou and Mingshan formations, as well as the common phosphate nodules in the lower part of the SRDs, characterise the T1 transgression (Fig. 14F, G). Similar to that in the northern part of the YCP, this transgression in the platform interior is marked by the occurrence of chert-bearing layers or marlstone at Luojiachong of an ICP from the LYR (Fig. 14F), as well as at Qixingjie and Cihua from the eastern part of the YCP (Fig. 14G). The return of shallow platform limestone to these sections during the Wordian corresponds to the R1 regression (Fig. 14F, G).

The R1 regression is clearly seen in the Cathaysian region as the progradation of siliciclastic deposits: delta-front sandstone at Lengwu (Fig. 14F) (Feng, 1991), and coal-bearing coastal siltstone and sandstone at Subang and Xinfeng (Fig. 14G). Basinwards, this regression is evidenced by SRDs being replaced by manganese carbonates in the Yongxing section (Fig. 14G).

The subsequent T2 transgression during the early-middle Capitanian is clearly developed in both platformal and paralic areas. At Luojiachong, Qixingjie and Cihua, the transition from shallow

832 platform limestone to SRDs characterises the T2 transgression in these carbonate platform settings
833 (Fig. 14F, G) (Wang, 1993; Wang, 1995b; Zeng et al., 2010). At Lengwu, Xinfeng and Subang, the
834 occurrences of marlstone and siltstone in the middle part of the Lengwu Formation, and SRDs of
835 the upper part of the Chetou and the middle part of the Tongziyan formations mark a fining trend
836 during T2 in these siliciclastic successions (Fig. 14F, G).

837 Above the T2 transgression, in carbonate systems, the R2 regression is marked by facies
838 changes to the bioherms (the upper part of the Maokou Formation at Luojiachong and the Wuxue
839 Formation at Yashan) surrounding an ICP from the LYR (Fig. 14F) (Luo et al., 1997) and to the
840 shallow platform carbonates at Qixingjie and Cihua on the eastern part of the YCP (Fig. 14G) (Wang,
841 1995b; Zeng et al., 2010). Meanwhile, in terrigenous settings, the R2 regression is the progradation
842 of terrestrial facies. The coarser-grained siliciclastics reached further Yangongtang, Zhengpanshan
843 and Chaohu in the LYR (Fig. 14F), and Yongxing in the Jiangnan Basin (Fig. 14G), indicating a
844 more substantial siliciclastic progradation than that of R1.

845 In eastern South China, the uppermost Guadalupian succession is either completely developed
846 or slightly eroded because of the late Guadalupian emergence (Hu, 1994; Zhang et al., 2019b). Thus,
847 it is hard to identify the spatial distribution of the T3 transgression. Some sections show potential
848 evidence: at Yongxing there is a change from sandstone to mudstone and at Qixingjie from platform
849 limestone to SRDs (Fig. 14G) (Wang, 1995b).

850

851 The discussions above illustrate that the Guadalupian sequence stratigraphy, identified at the
852 GSSP section of Tieqiao, is recognisable across all carbonate and siliciclastic depositional systems
853 in South China. Two regressions, R1 and R2, are recognised between three transgressions, T1, T2

and T3, constituting two and a half T-R sedimentary cycles. The first cycle T1-R1 spanned the early Roadian to the late Wordian. The second cycle T2-R2 occurred from the late Wordian to late Capitanian. The T3 transgression was present in the latest Capitanian.

6. Discussion

Having established a chronostratigraphic framework for the evolution of Guadalupian carbonate platforms in South China, we here discuss the interrelated factors that controlled the development of these platforms.

6.1 *Developing pattern of the YCP*

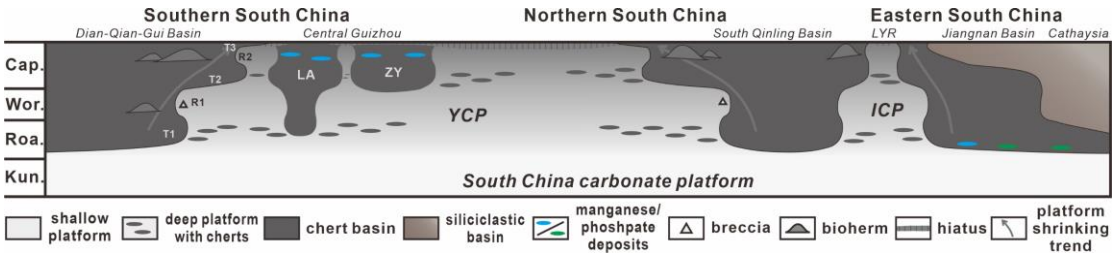

Fig. 15. Sketch showing carbonate platform evolution during the Guadalupian in different regions of South China. Abbreviations: Kun. - Kungurian; Roa. - Roadian; Wor. - Wordian; Cap. - Capitanian; LA - Liupanshui – Anshun area; ZY - Zunyi area.

Inherited from the late Kungurian, a shallow-water carbonate platform was still widespread during the earliest Guadalupian and termed the South China carbonate platform because it covered almost the entire region (Fig. 15) (Liu and Xu, 1994; Wang and Jin, 2000; Ma et al., 2009). However, a dramatic demise of the carbonate platform took place during the T1 transgression. As a result, the

874 initial YCP as well as some ICPs developed in the basins of the South Qinling region and the LYR,
875 replacing the South China carbonate platform (Figs. 1B, 15). Meanwhile, local intra-platform
876 depressions formed in the Liupanshui – Anshun area of central Guizhou (Fig. 15).

877 The YCP and ICPs contracted during the T2 transgression, when siliceous basins onlapped the
878 margins of the platforms, causing further area loss (Fig. 15). Within these platforms, the intra-
879 platform depressions expanded markedly in the Liupanshui – Anshun and Zunyi areas during T2.
880 Moreover, the deeper platform facies surrounding these basinal areas in the interior of the YCP also
881 developed at the expense of shallow platform facies (Figs. 1B, 15).

882 Following the above two transgressive phases respectively, the two expanding phases of
883 carbonate extent in our study interval saw the development of massive breccia and bioherms along
884 the peripheries of the YCP and ICPs (Fig. 15). The breccia, observed during the R1 regression,
885 indicates a shedding of the lithified YCP's margin. The bioherms mainly coincided with the R2
886 sequence which terminated at a regional unconformity. Notably, these bioherms developed enclosed
887 in slope or basinal environments and were probably independent of the broad platform area (Fig.
888 15). Thus, their occurrences in the preceding platform areas during the R1 regression, such as at
889 Rencunping and Luojiachong (Fig. 14E, F), demonstrate that the extents of the YCP and ICPs did
890 not recover to match those during R1 (Fig. 15).

891 After the R2 regression, a younger backstepping of platform carbonates occurred during T3,
892 although much of its distribution remains to be verified biostratigraphically in the platform margin
893 areas.

894 In summary, the YCP, which commenced after the drowning of the South China carbonate
895 platform, shrank during the Guadalupian as the platform margin contracted whereas deep-water

depressions developed within the platform interior (Fig. 15).

6.2 *Comparison to other Guadalupian carbonate platforms*

Marginal retreat accompanied with onlaps of the SRDs recorded in the YCP broadly occurs in other Guadalupian carbonate platforms worldwide.

The Permian Chert Event, corresponding to quantities of chert-bearing accumulation, formed a belt of glass ramps that substitute for carbonate production in many well-documented carbonate platform areas along the coast of boreal to tropical Pangea (Fig. 1A, locations 2-4) (Murchey and Jones, 1992; Ritterbush, 2019; Matheson and Frank, 2020a). The above substitution occurred simultaneously in the Phosphoria Sea and the Barents Sea during the Roadian (Blomeier et al., 2013; Davydov et al., 2018a; Matheson and Frank, 2020b) and emerged during the early Capitanian in the Sverdrup Basin (Beauchamp and Grasby, 2012). These two periods of substitution support the contraction of carbonate platforms associated with the T1 and T2 transgressions.

The subtropical to tropical paleo-Tethys is another region with thriving Guadalupian carbonate platforms (Fig. 1A). In the Arabian isolated platform and southern Primorye in Far East Russia (Fig. 1A, locations 5 and 9), the retreat of carbonate platform margins is evidenced by a facies shift from bioclastic limestone to mudstone or cherts in the upper part of the Guadalupian succession (Weidlich and Bernecker, 2007; Kani et al., 2018). Similar changes occur in Transcaucasia, the Abadeh area and the Pha Nok Khao platform (Fig. 1A, locations 6-8), where light grey, thick-bedded limestone becomes increasingly blackish and thinner, and contains a higher chert proportion upwards both in the middle and upper parts of the Capitanian succession, reflecting platform contraction during the T2 and T3 transgressions, respectively (Leven, 1998; Hada et al., 2015, fig. 4; Arefifard and Payne,

2020, fig. 10b).

In the Panthalassan paleo-atoll of southwest Japan (Fig. 1A, location 10), the marginal retreat has not been clearly observed on the seamount-capping carbonate mass, but the multiple subaerial exposures present in the carbonate interval during the Wordian and the late Capitanian could be attributed to the R1 and R2 regressions, respectively (Nakazawa and Ueno, 2004; Nakazawa et al., 2012; Kofukuda et al., 2014).

The measurement of the global lithofacies distribution by Kiessling et al. (2003) suggested that nearly 3×10^5 km^2 of shallow carbonate platform areas disappeared during the Guadalupian period. Comprehensive research of the process of Guadalupian platform contraction from platform to platform worldwide could undoubtedly be significant in revealing the mechanism of platform evolution. Nevertheless, the YCP could represent an irreplaceable case in this regard to be scrutinized for its complete Guadalupian succession and sound biostratigraphy basis.

6.3 *Regional tectonics on the carbonate platform evolution*

Demise of carbonate platforms is commonly attributed to increasing accommodation that can outpace platform growth, causing platform margins to retreat and give way to deeper-water facies (Godet, 2013; Menier et al., 2014). Rapid tectonic subsidence is one mechanism that may create accommodation and has generally been held responsible for SRDs development (*e.g.*, Kong and Gong, 1987; Feng, 1991; Jiang et al., 1994; Cheng et al., 2015). The ELIP was a major tectono-volcanic event in the western YCP region in the Middle to Late Permian. An “Emei taphrogenesis” was proposed to explain the occurrence of Emeishan basalts in narrow but thick (up to ~2000m) outcrops (Luo et al., 1988). The SRDs and manganese deposits in central Guizhou have long been

attributed to similar tectonic activities occurring in the western YCP region (Chen et al., 1984; Luo et al., 1988; Jin and Feng, 1995). However, other factors may be responsible for SRDs formation.

In this study, we have shown that, in central Guizhou, the SRDs were developed in depressions of various shapes and their distributions were scattered on the top of the YCP (Fig. 4B). These depressions do not show linear trends predicted by active, fault-controlled rifting (*e.g.*, Zhu et al., 1989; Chen et al., 2003). Such features imply that these depocentres were not the product of taphrogenesis. In addition, the gradational transition of lithofacies between shallow-water carbonates and deeper-water SRDs, with a belt of siliceous limestone transitional facies in-between (Fig. 1B), further argues against sharply delineated syn-rift basins (*e.g.*, Woodfine et al., 2010; Silva-Casal et al., 2019). The synchronous change in depositional facies of the platform margins, including areas surrounding the YCP and ICPs, and in the YCP's interior, also does not support a local, syndepositional faulting control on the occurrence of SRDs.

6.4 *Guadalupian environmental conditions for carbonate platform developing*

Anoxia and upwelling are two factors commonly discussed in the interpretation of Guadalupian marine environments in South China, and are interrelated to some extent. Their possible impacts on the YCP's evolution are discussed below.

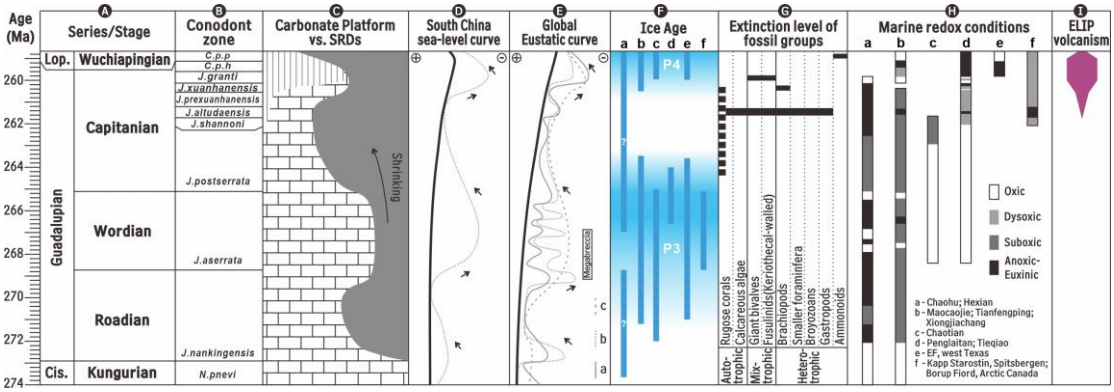

Fig. 16. Summary on the evolution of carbonate platforms in South China and possible influencing factors during Middle-Late Permian. (A, B) Timescale and biostratigraphic framework from Henderson (2016) and Shen et al. (2018). (C) Generalized platform margin onlaps based on this study. The interval filled by vertical lines shows missing strata caused by regression. (D) South China relative sea-level change modified from Wang et al. (1999). (E) Global eustatic sea-level changes modified from: a - Haq and Schutter (2008); b - Ross and Ross (1987); c - Haq and Al-Qahtani (2005). Megabreccia event from Haq and Schutter (2008). (F) Durations of glacial events. Data of a-d are from eastern Australia and recalibrated in this timescale based on: a - Fielding et al. (2008); b - Metcalfe et al. (2015); c - Frank et al. (2015); d - Garbelli et al. (2019). Data of e and f are from: e - NE Russia (Davydov et al., 2016; Davydov et al., 2018b); f - Arctic Canada (Beauchamp and Grasby, 2012). (G) Extinction levels of different fossil groups summarized from Wang and Sugiyama (2001), Weidlich (2002a), Ota and Isozaki (2006), Isozaki and Aljinović (2009), Shen and Shi (2009), Bond et al. (2010a) and Huang et al. (2018). (H) Comparison of marine redox conditions in: a - central Anhui (Wei et al., 2019; Zhang et al., 2019a); b - western Hubei (Shi et al., 2016; Wei et al., 2016) and central Guizhou (Wignall et al., 2009a); c - northern Sichuan (Saitoh et al., 2013b); d - central Guangxi (Zhang et al., 2015; Wei et al., 2016); e - West Texas (Zhang et al., 2015); f - Spitsbergen and Arctic Canada (Bond et al., 2015; Bond et al.,

2019). (I) Volcanism of the ELIP from Sun et al. (2010) and Wu et al. (2020).

Low oxygen (dysoxic) concentrations are commonly cited as a cause of impaired carbonate platform growth and may even cause platform shutdown, as documented by many Mesozoic examples (*e.g.*, Han et al., 2018; Jin et al., 2018; Bonvallet et al., 2019). In South China, dysoxic facies are common in the Guadalupian geological records. Thus, oxygen-deficient conditions were present in the Roadian recorded by the deposition of the Kuhfeng Formation, an organic rich shale with phosphate and manganese deposits (Tong and Zhou, 1985; Wu et al., 1994). Diverse indicators (*e.g.*, radiolarian palaeoecology, pyrite petrography and trace metal enrichment) indicate the Kuhfeng Formation was deposited in suboxic-euxinic conditions from the Roadian to early Capitanian, in basins surrounding the northern to eastern part of the YCP (Fig. 16H-a, b, c) (Saitoh et al., 2013b; Shi et al., 2016; Cao et al., 2018; Wei et al., 2019). In contrast, shallow-water areas remained oxygenated during this time (Wei et al., 2019).

Severe oxygen-deficiency occurred in the middle-late Capitanian, when the redox variation has been extensively investigated because of its potential role in the Capitanian extinction. Anoxic-euxinic conditions in the deep-water facies are evidenced by C-S-Fe systematics combined with enrichment of redox-sensitive trace element (Mo, U, V) contents in the LYR (Fig. 16H-a) (Zhang et al., 2019a), and by the small size of pyrite framboids in central Guizhou (Wignall et al., 2009a) and western Hubei (Fig. 16H-b) (Wei et al., 2016). At time these oxygen-poor conditions impinged in the northeastern margin of the YCP (Wei et al., 2019), and the southeastern margin of the Laibin – Heshan ICP (Fig. 16H-d) (Zhang et al., 2015).

Marine anoxia during the middle-late Capitanian was widespread and potentially a near-global

phenomenon, seen in tropical to temperate latitudes, including the Delaware Basin of western Pangea (Fig. 16H-e) (Zhang et al., 2015; Smith et al., 2019), the Sverdrup Basin (Arctic Canada) and the cool, temperate shelf seas (Spitsbergen) of northern Pangea (Fig. 16H-f) (Bond et al., 2015; Bond et al., 2019).

Therefore, recurrent dysoxic conditions in the basins surrounding carbonate platforms in South China may have affected the carbonate productivity of these areas, with upwelling exacerbating the effect (Saitoh et al., 2013a; Zhang et al., 2021). However, an upwelling mechanism is unlikely to have been important in the formation of the intra-platform depressions far removed from oceanic circulation regimes. Therefore, caution should be taken when invoking upwelling as a control on the entirety of carbonate platform evolution of the YCP in the Guadalupian.

6.5 *Glaciation*

Other than the regional factors discussed above, eustasy also plays a critical role in the construction of carbonate platforms (Pomar and Kendall, 2008). Glacio-eustasy is likely to have played a role in the development of Guadalupian carbonate systems of South China because the interval marked the final stages of the Late Paleozoic Ice Age (LPIA), the most prolonged glacial interval of the Phanerozoic.

The LPIA spanned the Carboniferous to Permian and saw ice caps develop, especially in southern hemisphere Gondwanan locations. Eight discrete glacial intervals (with interglacial intervals in-between) have been recognised (Fielding et al., 2008). Among the eight glaciations, the last two intervals, P3 and P4, occurred during the Middle-Late Permian and were initially identified in high-latitude glacial sedimentary records retrieved from eastern Australia (Fig. 16F-a) (Fielding

et al., 2008). In the Sydney and Bowen basins of eastern Australia, U-Pb CA-TIMS calibration of the glacial sedimentary formations suggests that P3 is late Roadian to early Capitanian in age, and P4 is latest Capitanian to Wuchiapingian in age (Fig. 16F-b) (Metcalfe et al., 2015). Based on the palaeotemperature proxies and sedimentological records in the same region, Frank et al. (2015) calibrated a slightly earlier P3 duration than that suggested by Metcalfe et al. (2015) (Fig. 16F-c). The recent $^{87}Sr/^{86}Sr$ ratio measured on brachiopod shells obtained from the Sydney Basin implied that the P3 duration is shorter than previously reported, extending only from the late Wordian to the early Capitanian (Fig. 16F-d) (Garbelli et al., 2019).

Sedimentary records from the northern hemisphere also confirm two glacial events in the Guadalupian. In the high-latitude NE Russia, the results of U-Pb dating on glacial sediments obtained by Davydov et al. (2016) and Davydov et al. (2018b) indicate that P3 spans the Wordian, and P4 is latest Capitanian to Wuchiapingian in age (Fig. 16F-e). In temperate regions, both glacial intervals coincide with the decrease of warm-water fusulinid diversity in North America (Davydov, 2014). Cooling in the Wordian was supported by the occurrence of a cool-water fauna of bryozoans and brachiopods, and dropstones in the Sverdrup Basin (Fig. 16F-f) (Beauchamp and Baud, 2002; Beauchamp and Grasby, 2012). In tropical South China, the P4 cooling interval has been conjectured from paleotemperature proxies during the earliest Wuchiapingian (Chen et al., 2013; Yang et al., 2018; Wang et al., 2020).

6.6 *Eustatic and relative sea-level changes*

The first order eustatic trend, derived from the study of depositional sequences of major cratons such as North America and Russian platform, consists of a regressive trend from the Roadian to the

1042 Wuchiapingian with amalgamation of the Pangea (Fig. 16E) (Ross and Ross, 1987; Haq and Al-
1043 Qahtani, 2005; Haq and Schutter, 2008). Second order changes, superimposed on this trend, consist
1044 of three intervals, all three dominated by sea-level rise, with two phases of regression. The former
1045 regression began during the late Roadian, after which the sea-level experienced a change to high
1046 frequency (third-order) fluctuations, with a magnitude up to approximately 70 m during the Wordian
1047 (Fig. 16E). This interval coincides with the P3 glaciation discussed above (Rygel et al., 2008; Chen
1048 et al., 2016) and well-developed lowstand features such as widespread carbonate megabreccias (Fig.
1049 16E) (Haq and Schutter, 2008). The latter regression during the late Capitanian marks one of the
1050 lowest points of sea-level in the Phanerozoic (Fig. 16E).

1051 The relative sea-level changes recorded in the Guadalupian succession of South China closely
1052 follow the eustatic trend. The Guadalupian succession in South China occurs beneath a major
1053 unconformity (Figs. 15, 16C) (Hou et al., 2020). This unconformity, first recognised in the 1930s,
1054 has been attributed to the "Dongwu tectonic movement" or "Dongwu uplift" (Hu, 1994) and marks
1055 the conventional lithostratigraphic boundary between the Guadalupian and Lopingian in China.
1056 Below the Guadalupian strata are the Chihsian carbonates and underlying thin coal-bearing littoral
1057 deposits (locally termed the Liangshan Formation and equivalents) (Fig. 3). There exists another
1058 major unconformity below the Liangshan Formation (Shen et al., 2018). The succession from the
1059 Liangshan Formation to the Chihsian carbonates constitutes a major transgressive sequence based
1060 on the succession from coal-bearing littoral deposits to shallow shelf carbonates with a major basal
1061 unconformity, as well as the widespread Chihsia Formation in the region. Thus, the entire
1062 Guadalupian succession in South China comprises the falling phase of a major sea-level change
1063 cycle, consistent with the regressive trend of the first order eustatic fluctuation (Fig. 16D, E) (Chen

et al., 1998; Mei et al., 1999; Shen et al., 2018). The minor cyclicity of the Guadalupian succession in South China, namely, the identified two and a half T-R cycles, also correlates well with the three intervals of the second order eustatic changes mentioned above (Wang et al., 1999; Hu et al., 2012) (Fig. 16D, E).

6.7 *Guadalupian mass extinction and carbonate factories*

The Guadalupian mass extinction has been demonstrated to be a global event (Shen and Shi, 2002; Clapham et al., 2009; Wignall et al., 2012; Bond et al., 2015), and recently ranked as the sixth major mass extinction (Rampino and Shen, 2019). It has been estimated that about 60% of species and 34% of genera of marine animals were eliminated during this biocrisis (Stanley, 2016). Photosynthetic and photosymbiont-bearing taxa, such as calcareous algae, keriothecal-walled fusulinids, alatoconchid bivalves and corals, were especially badly affected (Fig. 16G) (Isozaki and Aljinović, 2009; Wignall et al., 2009a). All of these taxa were important carbonate producers in the shallow platform environments of low-latitudes (Kiessling et al., 2003). During the crisis, reefs in the Guadalupian experienced a heavy loss in terms of both reef abundance and carbonate production, of 47% and 89% respectively (Flügel and Kiessling, 2002; Kiessling, 2002).

However, analysis of the geological literature suggests that reefs and carbonate platforms were generally two systems that were decoupled in quantity and quality (Kiessling et al., 2003). Reefs that flourished during the Guadalupian were mainly built by microbes, bryozoans and *Tubiphytes*, which had a minimal contribution to carbonate platforms (Kiessling, 2002; Weidlich, 2002b). If the shrinking process of the YCP shown above resulted from a less productive carbonate factory, then we must consider factors impacting the carbonate producers on the platform. As noted above, the

surrounding basinal areas were oxygen poor raising the possibility that such conditions may have reduced carbonate production. The loss of photosynthetic taxa during the Guadalupian mass extinction could also have played a role although the contraction in the area of platforms was underway long before the crisis (Fig. 16C, G). However, the timing of this crisis is debated and some have suggested there was a prolonged gradual pattern of diversity decline but no crisis event (Clapham et al., 2009; Groves and Wang, 2013). Cooling during glacial intervals is another possibility but it is noteworthy that the earlier glaciations of the Permian, before P3 and P4, did not impact carbonate productivity. Further work is clearly needed but it is noteworthy that neither scenario – abrupt crisis versus prolonged diversity decline – correlates closely with the waxing and waning of carbonate platform extent in the Guadalupian of South China (Fig 16).

7. Conclusion

1. A unique Guadalupian succession of deep-water SRDs, as well as manganese carbonates developed on the YCP in central Guizhou. Spatially, these SRDs developed in isolated depressions scattered in the region, surrounded by limestone of deeper platform facies. Conodont identification of this succession indicates that these deep-water deposits commenced in the Liupanshui – Anshun area during the Roadian and then spread northeastwards to the Zunyi area during the Capitanian.

2. Sequence correlations across the carbonate, siliceous and terrigenous depositional areas in South China reveal that there are three transgressions (T1, T2 and T3) and two regressions (R1 and R2) in the Guadalupian succession. The transgressive-regressive cycles match the Guadalupian global eustacy well.

3. The Guadalupian evolutionary history of the YCP in South China is recovered. The YCP

commenced during the early Guadalupian and thereafter experienced gradual contraction. The contraction process was demonstrated by the commencement and expansion of depositional depressions within the platform interior (partial drowning) and the increasing onlaps of the SRDs along the platform margin (marginal retreat).

4. The partial drowning and marginal retreat during the course of platform shrinking reminded us of less productive shallow-water carbonate factories on the platform top. In addition to the global eustatic fluctuations, attention should be given to the Guadalupian mass extinction and the environmental deterioration also potentially impacting the evolution of carbonate platforms during the Guadalupian.

Acknowledgements

We thank Die Chen for helpful field work, and Xia Wang and Bowen Zan for useful discussions to improve the manuscript. This work was supported by the National Natural Science Foundation of China (Grant No. 41872117 and No. 41472087). Zhichen Liu and Deng Chen's work was supported by the Young Talent Funding of Guizhou (No. 2019-5654). We gratefully acknowledge the constructive review by Merlynd Nestell and an anonymous reviewer for their thoughtful comments and suggestions that improved this manuscript.

Declaration of Competing Interest

The authors declared that they have no known competing financial interests or personal relationships that could have appeared to influence the work reported in this paper.

Appendix A. Supplementary data

Data of locations and total thickness of thin-bedded Guadalupian SRDs collected from the stratal sections in Guizhou Province.

Appendix B. Section information

Detailed information on sections for Guadalupian sequence correlation in South China

No.	Section	Location	Name of SRDs	Reference	Types of biostratigraphy
1	Shaiwa	Sidazhai, Ziyun, Guizhou	Linghao Fm.	Wang et al. (2016)	Conodont
2	Rencunping	Sangzhi, Hunan	Maokou Fm.	Cao et al. (2013); Cao et al. (2018)	Conodont
3	Zhengpanshan & Qinglongshan	Lungtan, Nanjing, Jiangsu	Kuhfeng Fm.	Jin (1960); Wang (1995a); Zhang et al. (2020)	Conodont
4	Chaohu (Anmenkou)	Chaohu, Anhui	Kuhfeng Fm.	Kametaka et al. (2005); Kametaka et al. (2009)	Radiolarian
5	Chaohu (Pingdingshan)	Chaohu, Anhui	Kuhfeng Fm.	Wang and Qi (1995); Wu et al. (2017); Zhang et al. (2019a); Zhang et al. (2019b)	Conodont; Radiolarian
6	Yangongtang	Jingxian, Anhui	Kuhfeng Fm.	Wang and Qi (1995); Du et al. (2010)	Radiolarian
7	Yashan	Nanling, Anhui	Kuhfeng Fm.	Luo et al. (1997); Du et al. (2010)	Radiolarian; Fusulinid
8	Tieqiao	Laibin, Guangxi	Maokou Fm.	Sha et al. (1990); Mei et al. (1999); Wang and Sugiyama (2001); Chen et al. (2009); Yao et al. (2012); Sun et al. (2017)	Conodont
9	Yanghe	Huaying, Sichuan	Maokou Fm.	Liu et al. (2016a)	Conodont
10	Maoershan/ Tianfengping	Enshi, Hubei	Maokou Fm.	Zhang et al. (2007)	Conodont

11	Shangsi	Guangyuan, Sichuan	Maokou Fm.	Lai et al. (2008); Sun et al. (2008)	Conodont
12	Nashui	Luodian, Guizhou	Maokou Fm.	Shi et al. (2000); Henderson and Mei (2003); Meng et al. (2018)	Conodont
13	Xiongjiachang	Zhijin, Guizhou	Maokou Fm.	Wignall et al. (2009a); Sun et al. (2010)	Conodont
14	Chaotian	Guangyuan, Sichuan	Maokou Fm.	Lai et al. (2008); Sun et al. (2008); Saitoh et al. (2013a); Saitoh et al. (2013b)	Conodont
15	Sancha	Zunyi, Guizhou	Maokou Fm.	This study	Conodont
16	Baiguowan	Zunyi, Guizhou	Maokou Fm.	This study	Conodont
17	Sangshuwan	Renhuai, Guizhou	Maokou Fm.	This study	Conodont
18	Shangji	Zunyi, Guizhou	Maokou Fm.	This study	Conodont
19	Pianpozhai	Shuicheng, Guizhou	Maokou Fm.	This study	Conodont
20	Yongxing	Chenzhou, Hunan	Maokou Fm.	Huang and Li (1992)	Conodont
21	Cihua	Yichun, Jiangxi	Nangang Fm.	Zeng et al. (2010)	Conodont
22	Maocaojie	Jianshi, Hubei	Kuhfeng Fm.	Shi et al. (2016)	Conodont
23	Nanjiang	Bazhong, Sichuan	Maokou Fm.	Mei et al. (1994)	Conodont
24	Luojiachong	Zhongming, Anhui	Kuhfeng Fm.	Wang (1993)	Conodont
25	Subang	Longyan, Fujian	Wenbishan Fm.	Li (2008)	Fusulinid
26	Xinfeng	Ganzhou, Jiangxi	Wenbishan Fm.	Liu (2008)	Fusulinid
27	Lengwu	Tonglu, Zhejiang	Dingjiashan Fm.	Wang (1993); Liu et al. (2016b)	Conodont

28	Chenxi	Huaihua, Hunan	Maokou Fm.	Mu et al. (1997)	No fossil record
29	Qixingjie	Lianyuan, Hunan	Maokou Fm.	Wang (1995b)	No fossil record
30	Heshan	Laibin, Guangxi	Maokou Fm.	Yu et al. (2016)	No fossil record
31	Liangshan	Hanzhong, Shaanxi	Maokou Fm.	Wang (1978); Kong (2011); Cao et al. (2018)	Conodont

References

Arefifard, S., 2017. Sea level drop, palaeoenvironmental change and related biotic responses across Guadalupian–Lopingian boundary in southwest, North and Central Iran. Geological Magazine 155, 1-23.

Arefifard, S., Payne, J.L., 2020. End-Guadalupian extinction of larger fusulinids in central Iran and implications for the global biotic crisis. Palaeogeography, Palaeoclimatology, Palaeoecology 550, 1-15.

Beauchamp, B., Baud, A., 2002. Growth and demise of Permian biogenic chert along northwest Pangea: evidence for end-Permian collapse of thermohaline circulation. Palaeogeography Palaeoclimatology Palaeoecology 184, 37-63.

Beauchamp, B., Grasby, S.E., 2012. Permian lysocline shoaling and ocean acidification along NW Pangea led to carbonate eradication and chert expansion. Palaeogeography Palaeoclimatology Palaeoecology 350-352, 73-90.

Blomeier, D., Dustira, A.M., Forke, H., Scheibner, C., 2013. Facies analysis and depositional environments of a storm-dominated, temperate to cold, mixed siliceous-carbonate ramp: The Permian Kapp Starostin Formation in NE Svalbard. Norsk Geologisk Tidsskrift 93, 75-93.

Bond, D.P.G., Hilton, J., Wignall, P.B., Ali, J.R., Stevens, L.G., Sun, Y.D., Lai, X.L., 2010a. The Middle Permian (Capitanian) mass extinction on land and in the oceans. Earth-Science Reviews 102, 100-116.

Bond, D.P.G., Wignall, P.B., Wang, W., Izon, G., Jiang, H.S., Lai, X.L., Sun, Y.D., Newton, R.J.,

1157 Shao, L.Y., Védrine, S., 2010b. The mid-Capitanian (Middle Permian) mass extinction and
1158 carbon isotope record of South China. Palaeogeography Palaeoclimatology Palaeoecology 292,
1159 282-294.
1160 Bond, D.P.G., Wignall, P.B., Joachimski, M., Sun, Y.D., Savov, I., Grasby, S., Beauchamp, B.,
1161 Blomeier, D., 2015. An abrupt extinction in the Middle Permian (Capitanian) of the Boreal
1162 Realm with a causal link to anoxia, acidification and mercury poisoning. Geological Society
1163 of America Bulletin 127, 1411-1421.
1164 Bond, D.P.G., Wignall, P.B., Grasby, S.E., 2019. The Capitanian (Guadalupian, Middle Permian)
1165 mass extinction in NW Pangea (Borup Fiord, Arctic Canada): A global crisis driven by
1166 volcanism and anoxia. GSA Bulletin 132, 931-942.
1167 Bonvallet, L., Arnaud-Vanneau, A., Arnaud, H., Adatte, T., Spangenberg, J.E., Stein, M., Godet, A.,
1168 Föllmi, K.B., 2019. Evolution of the Urgonian shallow-water carbonate platform on the
1169 Helvetic shelf during the late Early Cretaceous. Sedimentary Geology 387, 18-56.
1170 Bureau of Geology and Mineral Resources of Guizhou Province, 1987. Regional Geology Annals
1171 of Guizhou Province. Geological Publishing House, Beijing (in Chinese with English abstract).
1172 Bureau of Geology and Mineral Resources of Jiangxi Province, 1984. Regional Geology Annals of
1173 Jiangxi Province. Geological Publishing House, Beijing (in Chinese with English abstract).
1174 Cao, C.Q., Zhang, M.Y., Zheng, Q.F., Yuan, D.X., Chen, J., Ding, Y., 2013. The Permian Capitanian
1175 stratigraphy at the Rencunping Section, Sangzhi county of Hunan and its environmental
1176 implications. Journal of Stratigraphy 37, 485-498 (in Chinese with English abstract).
1177 Cao, C.Q., Cui, C., Chen, J., Summons, R.E., Shen, S.Z., Zhang, H., 2018. A positive C-isotope
1178 excursion induced by sea-level fall in the middle Capitanian of South China. Palaeogeography
1179 Palaeoclimatology Palaeoecology 505, 305-316.
1180 Catuneanu, O., Abreu, V., Bhattacharya, J., Blum, M., Dalrymple, R., Eriksson, P., Fielding, C.R.,
1181 Fisher, W., Galloway, W., Gibling, M., 2009. Towards the standardization of sequence
1182 stratigraphy. Earth-Science Reviews 92, 1-33.
1183 Cawood, P.A., Zhao, G.C., Yao, J.L., Wang, W., Xu, Y.J., Wang, Y.J., 2018. Reconstructing South
1184 China in Phanerozoic and Precambrian supercontinents. Earth-Science Reviews 186, 173-194.
1185 Chen, B., Joachimski, M.M., Shen, S.Z., Lambert, L.L., Lai, X.L., Wang, X.D., Chen, J., Yuan, D.X.,
1186 2013. Permian ice volume and palaeoclimate history: Oxygen isotope proxies revisited.

1187 Gondwana Research 24, 77-89.
1188 Chen, B., Joachimski, M.M., Wang, X.D., Shen, S.Z., Qi, Y.P., Qie, W.K., 2016. Ice volume and
1189 paleoclimate history of the Late Paleozoic Ice Age from conodont apatite oxygen isotopes from
1190 Naqing (Guizhou, China). Palaeogeography Palaeoclimatology Palaeoecology 448, 151-161.
1191 Chen, F.Y., Xue, W.Q., Yan, J.X., Wignall, P.B., Meng, Q., Luo, J.X., Feng, Q.L., 2018.
1192 Alatoconchids: Giant Permian bivalves from South China. Earth-Science Reviews 179, 147-
1193 167.
1194 Chen, W.Y., Wang, L.T., Ye, N.Z., Cai, Y., Ma, Z.W., Ling, C.F., 1984. A study of the Early Pemian
1195 lithofacies and paleogeographical map of Guizhou. Geology of Kuichow 1, 9-64 (in Chinese
1196 with English abstract).
1197 Chen, W.Y., Liu, J.R., Wang, Z.G., Zheng, Q.Q., 2003. Study on lithofacies palaeogeography during
1198 the Permian Emeishan Basalt explosion in Guizhou Province. Journal of Palaeogeography 5,
1199 17-28 (in Chinese with English abstract).
1200 Chen, Z.L., Shen, A.J., Jin, S.Y., Ju, T.Y., 1995. Diagenesis of the reefs of Tubiphytes - leaflike algea
1201 at Maokou Stage in Tongling, Anhui. South China Petroleum Geology 1, 19-24 (in Chinese
1202 with English abstract).
1203 Chen, Z.Q., Jin, Y.G., Shi, G.R., 1998. Permian transgression-regression sequences and sea-level
1204 changes of South China. Proceedings of Royal Society of Victoria 110, 345-367.
1205 Chen, Z.Q., George, A.D., Yang, W.R., 2009. Effects of Middle–Late Permian sea-level changes
1206 and mass extinction on the formation of the Tieqiao skeletal mound in the Laibin area, South
1207 China. Australian Journal of Earth Sciences 56, 745-763.
1208 Cheng, C., Li, S.Y., Zhao, D.Q., Yan, L., 2015. Geochemical characteristics of the Middle-Upper
1209 Permian bedded cherts in the northern margin of the Yangtze Blocks and its response to the
1210 evolution of paleogeography and paleo-ocean. Bulletin of Mineralogy, Petrology and
1211 Geochemistry 31, 155-166 (in Chinese with English abstract).
1212 Cheng, C., Li, S.Y., Cao, T.L., 2017. Permian Condonts at the Xikou Section, Zheng'an, Shaanxi
1213 Province, NW China. Acta Micropalaeontologica Sinica 34, 16-32 (in Chinese with English
1214 abstract).
1215 Clapham, M.E., Shen, S.Z., Bottjer, D.J., 2009. The double mass extinction revisited: reassessing
1216 the severity, selectivity, and causes of the end-Guadalupian biotic crisis (Late Permian).

1217 Paleobiology 35, 32-50.
1218 Clapham, M.E., Payne, J.L., 2011. Acidification, anoxia, and extinction: A multiple logistic
1219 regression analysis of extinction selectivity during the Middle and Late Permian. Geology 39,
1220 1059-1062.
1221 Davydov, V.I., 2014. Warm water benthic foraminifera document the Pennsylvanian–Permian
1222 warming and cooling events - The record from the Western Pangea tropical shelves.
1223 Palaeogeography Palaeoclimatology Palaeoecology 414, 284-295.
1224 Davydov, V.I., Biakov, A.S., Isbell, J.L., Crowley, J.L., Schmitz, M.D., Vedernikov, I.L., 2016.
1225 Middle Permian U–Pb zircon ages of the "glacial" deposits of the Atkan Formation, Ayan-
1226 Yuryakh anticlinorium, Magadan province, NE Russia: Their significance for global climatic
1227 interpretations. Gondwana Research 38, 74-85.
1228 Davydov, V.I., Crowley, J.L., Schmitz, M.D., Snyder, W.S., 2018a. New U–Pb constraints identify
1229 the end-Guadalupian and possibly end-Lopingian extinction events conceivably preserved in
1230 the passive margin of North America: implication for regional tectonics. Geological Magazine
1231 155, 119-131.
1232 Davydov, V.I., Biakov, A.V., Schmitz, M.D., Silantiev, V.V., 2018b. Radioisotopic calibration of the
1233 Guadalupian (middle Permian) series: Review and updates. Earth-Science Reviews 176, 222-
1234 240.
1235 Du, X., Zhang, Y.K., 1998. Regional Stratigraphy of Southeast China. China University of
1236 Geosciences Press, Wuhan, Hubei (in Chinese with English abstract).
1237 Du, Y.L., Li, S.Y., Kong, W.L., Li, H.X., 2010. The Permian sedimentary facies and depositional
1238 environment analysis in the Jingxian-Nanling region of Anhui. Journal of Stratigraphy 34, 431-
1239 444 (in Chinese with English abstract).
1240 Fan, J.X., Shen, S.Z., Erwin, D.H., Sadler, P.M., MacLeod, N., Cheng, Q.M., Hou, X.D., Yang, J.,
1241 Wang, X.D., Wang, Y., Zhang, H., Chen, X., Li, G.X., Zhang, Y.C., Shi, Y.K., Yuan, D.X.,
1242 Chen, Q., Zhang, L.N., Li, C., Zhao, Y.Y., 2020. A high-resolution summary of Cambrian to
1243 Early Triassic marine invertebrate biodiversity. Science 367, 272-277.
1244 Feng, Z.Z., 1991. Lithofacies Paleogeography of Permian of Middle and Lower Yangtze Region.
1245 Geological Publishing House, Beijing (in Chinese with English abstract).
1246 Feng, Z.Z., Yang, Y.Q., Jin, Z.K., He, Y.B., Wu, S.H., Xin, W.J., Bao, Z.D., Tan, J., 1996. Lithofacies

paleogeography of the Permian of South China. Acta Sedimentologica Sinica 14, 1-11 (in Chinese with English abstract).

Fielding, C.R., Frank, T.D., Birgenheier, L.P., Rygel, M.C., Jones, A.T., Roberts, J., 2008. Stratigraphic imprint of the Late Paleozoic Ice Age in eastern Australia: A record of alternating glacial and nonglacial climate regime. Journal of the Geological Society 165, 129-140.

Flügel, E., Kiessling, W., 2002. Patterns of Phanerozoic Reef Crises, in: Kiessling, W., Flügel, E., Golonka, J. (Eds.), Phanerozoic Reef Patterns. Society for Sedimentary Geology, Tulsa, pp. 691-733.

Flügel, E., 2010. Recognizing Paleoenvironmental Conditions, in: Flügel, E. (Ed.), Microfacies of Carbonate Rocks: Analysis, Interpretation and Application. Springer-Verlag, Berlin, Heidelberg, pp. 587-640.

Frank, T.D., Shultis, A.I., Fielding, C.R., 2015. Acme and demise of the late Palaeozoic ice age: A view from the southeastern margin of Gondwana. Palaeogeography Palaeoclimatology Palaeoecology 418, 176-192.

Garbelli, C., Shen, S.Z., Immenhauser, A., Brand, U., Buhl, D., Wang, W.Q., Zhang, H., Shi, G.R., 2019. Timing of Early and Middle Permian deglaciation of the southern hemisphere: Brachiopod-based $^{87}Sr/^{86}Sr$ calibration. Earth and Planetary Science Letters 516, 122-135.

Godet, A., 2013. Drowning unconformities: Palaeoenvironmental significance and involvement of global processes. Sedimentary Geology 293, 45-66.

Groves, J.R., Wang, Y., 2013. Timing and size selectivity of the Guadalupian (Middle Permian) fusulinoidean extinction. Journal of Paleontology 87, 183-196.

Hada, S., Khosithanont, S., Goto, H., Fontaine, H., Salyapongse, S., 2015. Evolution and extinction of Permian fusulinid fauna in the Khao Tham Yai Limestone in NE Thailand. Journal of Asian Earth Sciences 104, 175-184.

Hallam, A., Wignall, P.B., 1999. Mass extinctions and sea-level changes. Earth-Science Reviews 48, 217-250.

Han, Z., Hu, X.M., Kemp, D.B., Li, J., 2018. Carbonate-platform response to the Toarcian Oceanic Anoxic Event in the southern hemisphere: Implications for climatic change and biotic platform demise. Earth and Planetary Science Letters 489, 59-71.

Haq, B.U., Al-Qahtani, A.M., 2005. Phanerozoic cycles of sea-level change on the Arabian Platform.

GeoArabia 10, 127-160.

Haq, B.U., Schutter, S.R., 2008. A chronology of Paleozoic sea-Level changes. Science 322, 64-68.

He, B., Xu, Y.G., Chung, S.L., Xiao, L., Wang, Y., 2003. Sedimentary evidence for a rapid, kilometre scale crustal doming prior to the eruption of the Emeishan flood basalts. Earth Planet Sci Lett. Earth and Planetary Science Letters 213, 391-405.

He, L.X., He, F.R., 1953. General survey of manganese ore in southeastern Zunyi, Guizhou (in Chinese).

Henderson, C.M., Mei, S., 2003. Stratigraphic versus environmental significance of Permian serrated conodonts around the Cisuralian–Guadalupian boundary: new evidence from Oman. Palaeogeography Palaeoclimatology Palaeoecology 191, 301-328.

Henderson, C.M., 2016. Permian conodont biostratigraphy. Geological Society, London, Special Publications 450, 119-142.

Hou, Z.S., Fan, J.X., Henderson, C.M., Yuan, D.X., Shen, B.H., Wu, J., Wang, Y., Zheng, Q.F., Zhang, Y.C., Wu, Q., Shen, S.Z., 2020. Dynamic palaeogeographic reconstructions of the Wuchiapingian Stage (Lopingian, Late Permian) for the South China Block. Palaeogeography Palaeoclimatology Palaeoecology 546, 1-18.

Hu, M.Y., Hu, Z.G., Wei, G.Q., Yang, W., Liu, M.C., 2012. Sequence lithofacies paleogeography and reservoir potential of the Maokou Formation in Sichuan Basin. Petroleum Exploration and Development 39, 51-61.

Hu, S.Z., 1994. On the event of Dongwu Movement and its relation with Permian subdivision. Journal of stratigraphy 18, 309-315 (in Chinese with English abstract).

Huang, Y., Li, D.H., 1992. Discovery of Pemian condont from Lianyang coal field and its significance. Coal Geology of China 4, 6-11 (in Chinese with English abstract).

Huang, Y.G., Chen, Z.Q., Zhao, L.S., Jr George, D.S., Yan, J.X., Pei, Y., Yang, W.R., Huang, J.H., 2017. Restoration of reef ecosystems following the Guadalupian–Lopingian boundary mass extinction: Evidence from the Laibin area, South China. Palaeogeography Palaeoclimatology Palaeoecology 519, 8-22.

Huang, Y.G., Chen, Z.Q., Wignall, P.B., Grasby, S.E., Zhao, L.S., Wang, X.D., Kaiho, K., 2018. Biotic responses to volatile volcanism and environmental stresses over the Guadalupian-Lopingian (Permian) transition. Geology 47, 175-178.

1307 Isozaki, Y., 1997. Permo-Triassic Boundary Superanoxia and Stratified Superocean: Records from
1308 Lost Deep Sea. Science 276, 235-238.
1309 Isozaki, Y., Kawahata, H., Minoshima, K., 2007. The Capitanian (Permian) Kamura cooling event:
1310 The beginning of the Paleozoic–Mesozoic transition. Palaeoworld 16, 16-30.
1311 Isozaki, Y., Aljinović, D., 2009. End-Guadalupian extinction of the Permian gigantic bivalve
1312 Alatoconchidae: End of gigantism in tropical seas by cooling. Palaeogeography
1313 Palaeoclimatology Palaeoecology 284, 11-21.
1314 Jiang, N.Y., Jia, R., Wang, Z., Qi, D., Yu, Z., He, Y., 1994. Permian Palaeogeography and
1315 Geochemical Environment in Lower Yangtze Region, China. Petroleum Industry Press,
1316 Beijing (in Chinese with English abstract).
1317 Jin, X., Shi, Z.Q., Rigo, M., Franceschi, M., Preto, N., 2018. Carbonate platform crisis in the Carnian
1318 (Late Triassic) of Hanwang (Sichuan Basin, South China): Insights from conodonts and stable
1319 isotope data. Journal of Asian Earth Sciences 164, 104-124.
1320 Jin, Y.G., 1960. Conodonts from the Kufeng Suite (Formation) of Lungtan, Nanking. Acta
1321 Palaeontologica Sinica 8, 230-248 (in Chinese with English abstract).
1322 Jin, Y.G., Zhang, J., Shang, Q.H., 1994. Two phases of the end-Permian mass extinction. Canadian
1323 Society of Petroleum Geologists Memoir 17, 813-822.
1324 Jin, Y.G., Bruce, R.W., Brian, F.G., Galian, V.K., 1997. Permian chronostratigraphic subdivisions.
1325 Episodes 20, 10-15.
1326 Jin, Y.G., Shen, S.Z., Henderson, C.M., Wang, X.D., Wang, W., Wang, Y., Cao, C.Q., Shang, Q.H.,
1327 2006. The Global Stratotype Section and Point (GSSP) for the boundary between the
1328 Capitanian and Wuchiapingian stage (Permian). Episodes 29, 253-262.
1329 Jin, Z.K., Feng, Z.Z., 1995. Platform depression of the Permian of Guizhou Province and its
1330 comparison with platforms and basins. Acta Sedimentologica Sinica 90, 1230-1232 (in
1331 Chinese with English abstract).
1332 Kametaka, M., Takebe, M., Nagai, H., Zhu, S.Z., Takayanagi, Y., 2005. Sedimentary environments
1333 of the Middle Permian phosphorite–chert complex from the northeastern Yangtze platform,
1334 China; the Gufeng Formation: a continental shelf radiolarian chert. Sedimentary Geology 174,
1335 197-222.
1336 Kametaka, M., Nagai, H., Zhu, S.Z., Takebe, M., 2009. Middle Permian radiolarians from

1337 Anmenkou, Chaohu, Northeastern Yangtze platform, China. Island Arc 18, 108-125.
1338 Kani, T., Isozaki, Y., Hayashi, R., Zakharov, Y., Popov, A., 2018. Middle Permian (Capitanian)
1339 seawater 87 Sr/ 86 Sr minimum coincided with disappearance of tropical biota and reef
1340 collapse in NE Japan and Primorye (Far East Russia). Palaeogeography Palaeoclimatology
1341 Palaeoecology 499, 13-21.
1342 Kiessling, W., Flugel, E., Golonka, J., 2000. Fluctuations in the carbonate production of Phanerozoic
1343 reefs. Geological Society London Special Publications 178, 191-215.
1344 Kiessling, W., 2002. Secular variations in the Phanerozoic reef ecosystem, in: Kiessling, W., Flügel,
1345 E., Golonka, J. (Eds.), Phanerozoic Reef Patterns. SEPM Society for Sedimentary Geology,
1346 pp. 625-690.
1347 Kiessling, W., Flügel, E., Golonka, J., 2003. Patterns of Phanerozoic carbonate platform
1348 sedimentation. Lethaia 36, 195-225.
1349 Kong, Q.Y., Gong, Y.J., 1987. The formation environment of the Lower Permian radiolarian
1350 siliciliths in Jiangsu-Anhui region. Oil and Gas Geology 8, 86-89 (in Chinese with English
1351 abstract).
1352 Kong, W.L., 2011. Research of Sedimentary Facies and Paleogeography of Middle and Late
1353 Permian in the Northern Margin of Middle and Upper Yangtze Region. Hefei University of
1354 Technology (in Chinese with English abstract).
1355 Lai, X.L., Wang, W., Wignall, P.B., Bond, D.P.G., Jiang, H.S., Ali, J.R., John, E.H., Sun, Y.D., 2008.
1356 Palaeoenvironmental change during the end-Guadalupian (Permian) mass extinction in
1357 Sichuan, China. Palaeogeography Palaeoclimatology Palaeoecology 269, 78-93.
1358 Leven, E.J.A., 1998. Permian fusulinid assemblages and stratigraphy of the transcaucasia. Rivista
1359 Italiana Di Paleontologia E Stratigrafia 104, 299-328.
1360 Li, J.H., 2008. Lithostratigraphy of Fujian Province. China University of Geosciences Press, Wuhan,
1361 Hubei (in Chinese with English abstract).
1362 Liu, B.J., Xu, X.S., 1994. Atlas of the Lithofacies and Palaeogeography of South China (Sinian-
1363 Triassic). Science Press, Beijing (in Chinese).
1364 Liu, C., Fang, Q., Jing, X.C., 2016a. Study of the conodont biostratigraphy and color alternation
1365 index in the Permian Maokou Formation from the mid-Eastern Sichuan Basin, Southwest
1366 China. Acta Micropalaeontologica Sinica 33, 9-20 (in Chinese with English abstract).

1367 Liu, L., Wu, Y.S., Jiang, H.X., Liu, H., 2016b. Growth characteristics and sedimentary mode of
1368 Permian reefs, Lengwu, Tonglu, Zhejiang Province, southern China. Journal of
1369 Palaeogeography 5, 409-422.
1370 Liu, X.F., Wang, Q.S., Gao, X.J., 1989. Manganese Deposits of Guizhou, China Guizhou People's
1371 Publishing House, Guiyang (in Chinese with English abstract).
1372 Liu, X.T., Yan, J.X., 2009. A review of influences of seawater chemical evolution on
1373 biomineralization. Journal of Palaeogeography 11, 446-454 (in Chinese with English abstract).
1374 Liu, Y.G., 2008. Lithostratigraphy of Jiangxi Province. China University of Geosciences Press,
1375 Wuhan, Hubei (in Chinese with English abstract).
1376 Luo, X.M., Xu, G.R., Chen, L.Z., Huang, S.J., 1997. Sedimentary characsteristics of the Wuxue
1377 Formation in the Susong-Fanchang region, Anhui. Sedimentary Facies and Palaeogeography
1378 17, 19-27 (in Chinese with English abstract).
1379 Luo, Z.L., Jin, Y.Z., Zhu, K.Y., Zhao, X.K., 1988. On Emei taphrogenesis of the upper Yangtze
1380 platform. Geological Review 34, 11-24 (in Chinese with English abstract).
1381 Ma, Q.F., Feng, Q.L., Caridroit, M., Danelian, T., Zhang, N., 2016. Integrated radiolarian and
1382 conodont biostratigraphy of the Middle Permian Gufeng Formation (South China). Comptes
1383 Rendus Palevol 15, 453-459.
1384 Ma, Y.S., Chen, H.D., Wang, G.L., 2009. Tectonic-Sequence-Based Lithofacies and Paleogeography
1385 Atlas in South China, in: Ma, Y.S., Chen, H.D., Wang, G.L. (Eds.). Science Press, Beijing, p.
1386 (in Chinese).
1387 Matheson, E.J., Frank, T.D., 2020a. An epeiric glass ramp: Permian low-latitude neritic siliceous
1388 sponge colonization and its novel preservation (Phosphoria Rock Complex). Sedimentary
1389 Geology 399, 1-22.
1390 Matheson, E.J., Frank, T.D., 2020b. Phosphorites, glass ramps and carbonate factories: The
1391 evolution of an epicontinental sea and a late Palaeozoic upwelling system (Phosphoria Rock
1392 Complex). Sedimentology 67, 1-39.
1393 McGhee, J.G.R., Clapham, M.E., Sheehan, P.M., Bottjer, D.J., Droser, M.L., 2013. A new
1394 ecological-severity ranking of major Phanerozoic biodiversity crises. Palaeogeography
1395 Palaeoclimatology Palaeoecology 370, 260-270.
1396 Mei, S.L., Jin, Y.G., Wardlaw, B.R., 1994. Zonation of conodont from the Maokouan-

1397 Wuchiapingian boundary strata, South China. Palaeoworld 4, 225-233.
1398 Mei, S.L., Shi, X.Y., Chen, X.F., Sun, K.Q., Yan, J.X., 1999. Permian Cisuralian and Guadalupian
1399 sequence stratigraphy in south Guizhou and central Guangxi and its relation to conodont
1400 evolution. Earth Science-Journal of China University of Geosciences 24, 21-31 (in Chinese
1401 with English abstract).
1402 Meng, Q., Huang, H., Yan, J.X., Chen, F.Y., 2018. Sedimentary evolution of the Middle Permian
1403 carbonate platform margin in sounthern Guizhou and its palaeo-oceanographic implications.
1404 Journal of Palaeogeography 20, 87-103 (in Chinese with English abstract).
1405 Menier, D., Pierson, B., Chalabi, A., Ting, K.K., Pubellier, M., 2014. Morphological indicators of
1406 structural control, relative sea-level fluctuations and platform drowning on present-day and
1407 Miocene carbonate platforms. Marine and Petroleum Geology 58, 776-788.
1408 Metcalfe, I., 2013. Gondwana dispersion and Asian accretion: Tectonic and palaeogeographic
1409 evolution of eastern Tethys. Journal of Asian Earth Sciences 66, 1-33.
1410 Metcalfe, I., Crowley, J.L., Nicoll, R.S., Schmitz, M., 2015. High-precision U-Pb CA-TIMS
1411 calibration of Middle Permian to Lower Triassic sequences, mass extinction and extreme
1412 climate-change in eastern Australian Gondwana. Gondwana Research 28, 61-81.
1413 Moore, C.H., Wade, W.J., 2013. The Impact of Global Tectonics and Biologic Evolution on the
1414 Carbonate System, in: Moore, C.H., Wade, W.J. (Eds.), Developments in Sedimentology.
1415 Elsevier, Amsterdam, pp. 39-48.
1416 Mu, C.L., Qiu, D.Z., Wang, L.Q., Wan, F., 1997. Permian sedimentary basins and sequence
1417 stratigraphy in the Hunan-Hubei-Jiangxi region. Sedimentary Facies and Palaeogeography 17,
1418 1-26 (in Chinese with English abstract).
1419 Murchey, B.L., Jones, D.L., 1992. A mid-Permian chert event: widespread deposition of biogenic
1420 siliceous sediments in coastal, island arc and oceanic basins. Palaeogeography
1421 Palaeoclimatology Palaeoecology 96, 161-174.
1422 Ota, A., Isozaki, Y., 2006. Fusuline biotic turnover across the Guadalupian-Lopingian (Middle-
1423 upper Permian) boundary in mid-oceanic carbonate buildups: Biostratigraphy of accreted
1424 limestone in Japan. Journal of Asian Earth Sciences 26, 353-368.
1425 Phelps, R.M., Kerans, C., Rui, D.G., Jeremiah, J., Hull, D., Loucks, R.G., 2015. Response and
1426 recovery of the Comanche carbonate platform surrounding multiple Cretaceous oceanic anoxic

events, northern Gulf of Mexico. Cretaceous Research 54, 117-144.

Pomar, L., Kendall, C., 2008. Architecture of Carbonate Platforms: A Response to Hydrodynamics and Evolving Ecology, in: Lukasik, J., Simo, J.A. (Eds.), Controls on Carbonate Platform and Reef Development. SEPM Special Publication, Tulsa, pp. 187-216.

Rampino, M., Shen, S.Z., 2019. The end-Guadalupian (259.8 Ma) biodiversity crisis: the sixth major mass extinction? Historical Biology 33, 1-7.

Regional Geological Survey Report, 1971. Regional Geological Survey Report of the People's Republic of China (Shuicheng District, Zunyi District, Bijie District; 1: 200 000), Guiyang (in Chinese).

Ritterbush, K., 2019. Sponge meadows and glass ramps: State shifts and regime change. Palaeogeography, Palaeoclimatology, Palaeoecology 513, 116-131.

Ross, C.A., Ross, J.R., 1987. Late Paleozoic sea levels and depositional sequences. Cushman Foundation for Foraminiferal Research 24, 137-149.

Rygel, M.C., Fielding, C.R., Frank, T.D., Birgenheier, L.P., 2008. The Magnitude of Late Paleozoic Glacioeustatic Fluctuations: A Synthesis. Journal of Sedimentary Research 78, 500-511.

Saitoh, M., Isozaki, Y., Ueno, Y., Yoshida, N., Yao, J.X., Ji, Z.S., 2013a. Middle–Upper Permian carbon isotope stratigraphy at Chaotian, South China: Pre-extinction multiple upwelling of oxygen-depleted water onto continental shelf. Journal of Asian Earth Sciences 67-68, 51-62.

Saitoh, M., Isozaki, Y., Yao, J.X., Ji, Z.S., Ueno, Y., Yoshida, N., 2013b. The appearance of an oxygen-depleted condition on the Capitanian disphotic slope/basin in South China: Middle–Upper Permian stratigraphy at Chaotian in northern Sichuan. Global and Planetary Change 105, 180-192.

Schlager, W., 2003. Benthic carbonate factories of the Phanerozoic. International Journal of Earth Sciences 92, 445-464.

Scotese, C.R., 2014. Atlas of Middle & Late Permian and Triassic Paleogeographic maps, maps 43–48 from volume 3 of the PALEOMAP Atlas for ArcGIS (Jurassic and Triassic) and maps 49–52 from volume 4 of the PALEOMAP PaleoAtlas for ArcGIS (Late Paleozoic). Mollweide Projection, PALEOMAP Project, Evanston, IL.

Sha, Q.A., Wu, W.S., Fu, J.M., 1990. An Integrated Investigation on the Permian System of Qin-Gui Areas,With Discussion on Hydrocarbon Potential. Science Press, Beijing (in Chinese with

English abstract).

Shen, S.Z., Shi, G.R., 2002. Paleobiogeographical extinction patterns of Permian brachiopods in the Asian-western Pacific region. Paleobiology 28, 449-463.

Shen, S.Z., Shi, G.R., 2009. Latest Guadalupian brachiopods from the Guadalupian/Lopingian boundary GSSP section at Penglaitan in Laibin, Guangxi, South China and implications for the timing of the pre-Lopingian crisis. Palaeoworld 18, 152-161.

Shen, S.Z., Zhang, H., Zhang, Y.C., Yuan, D.X., Chen, B., He, W.H., Mu, L., Lin, W., Wang, W.Q., Chen, J., 2018. Permian integrative stratigraphy and timescale of China. Science China Earth Sciences 62, 1-35.

Shen, S.Z., Yuan, D.X., Henderson, C.M., Wu, Q., Zhang, Y.C., Zhang, H., Mu, L., Ramezani, J., Wang, X.D., Lambert, L.L., Erwin, D.H., Hearst, J.M., Xiang, L., Chen, B., Fan, J.X., Wang, Y., Wang, W.Q., Qi, Y.P., Chen, J., Qie, W.K., Wang, T.T., 2020. Progress, problems and prospects: An overview of the Guadalupian Series of South China and North America. Earth-Science Reviews 211, 1-26.

Sheng, J.Z., Jin, Y.G., 1994. Correlation of Permian Deposits in China. Palaeoworld 4, 14-113.

Shi, G.R., Shen, S.Z., Tong, J.N., 1999. Two discrete, possibly unconnected, Permian marine mass extinctions, pp. 148-150.

Shi, L., Feng, Q.l., Shen, J., Ito, T., Chen, Z.Q., 2016. Proliferation of shallow-water radiolarians coinciding with enhanced oceanic productivity in reducing conditions during the Middle Permian, South China: evidence from the Gufeng Formation of western Hubei Province. Palaeogeography Palaeoclimatology Palaeoecology 444, 1-14.

Shi, X.Y., Mei, S.L., Sun, Y., 2000. Permian sequence stratigraphy of slope facies in southern Guizhou and chronostratigraphic correlation. Science China Earth Sciences 43, 63-76.

Silva-Casal, R., Aurell, M., Payros, A., Pueyo, E.L., Serra-Kiel, J., 2019. Carbonate ramp drowning caused by flexural subsidence: The South Pyrenean middle Eocene foreland basin. Sedimentary Geology 393-394, 1-23.

Smith, B.P., Larson, T., Martindale, R.C., Kerans, C., 2019. Impacts of basin restriction on geochemistry and extinction patterns: A case from the Guadalupian Delaware Basin, USA. Earth and Planetary Science Letters 530, 1-11.

Stanley, S.M., Yang, X.N., 1994. A Double Mass Extinction at the End of the Paleozoic Era. Science

266, 1340-1344.

Stanley, S.M., 2016. Estimates of the magnitudes of major marine mass extinctions in earth history. Proceedings of the National Academy of Sciences 133, E6325-E6334.

Sun, Y.D., Lai, X.L., Jiang, H.S., Luo, G.M., Sun, S., Yan, C.B., Wignall, P.B., 2008. Guadalupian (Middle Permian) Conodont Faunas at Shangsi Section, Northeast Sichuan Province. Journal of China University of Geosciences 19, 451-460.

Sun, Y.D., Lai, X.L., Wignall, P.B., Widdowson, M., Ali, J.R., Jiang, H.S., Wang, W., Yan, C.B., Bond, D.P.G., Védrine, S., 2010. Dating the onset and nature of the Middle Permian Emeishan large igneous province eruptions in SW China using conodont biostratigraphy and its bearing on mantle plume uplift models. Lithos 119, 20-33.

Sun, Y.D., Liu, X.T., Yan, J.X., Li, B., Chen, B., Bond, D.P.G., Joachimski, M.M., Wignall, P.B., Wang, X., Lai, X.L., 2017. Permian (Artinskian to Wuchapingian) conodont biostratigraphy in the Tieqiao section, Laibin area, South China. Palaeogeography Palaeoclimatology Palaeoecology 465, 43-63.

Tian, W.X., Zhang, H.J., Li, X.W., Gong, Z.Y., Li, Z.H., 2007. The Permian sequence sequence stratigraphy and basin evolution in southwest of Hubei. Resource Enviornment and Engineering 21, 95-100 (in Chinese with English abstract).

Tong, Y.M., Zhou, Z.X., 1985. Preliminary study on the origin of the radiolaria-bearing siliceous rocks of Maokou Formation (Lower Permian), Southeast Hubei Province. Acta Sedimentologica Sinica 3, 67-74 (in Chinese with English abstract).

Ueno, K., Shi, G.R., Shen, S.Z., 2005. Fusulinoideans from the early Midian (late Middle Permian) *Metadoliolina dutkevitchi-Monodiexodina sutchanica* Zone of the Senkina Shapka section, South Primorye, Far East Russia. Alcheringa: An Australasian Journal of Palaeontology 29, 257-273.

Wan, T.F., 2012. The Tectonics of China: Data, Maps and Evolution. Springer-Verlag, Berlin, Heidelberg.

Wang, C.S., Li, X.H., Chen, H.D., Qin, J.X., 1999. Permian sea-level changes and rising-falling events in South China. Acta Sedimentologica Sinica 17, 536-541 (in Chinese with English abstract).

Wang, C.Y., 1993. Conodonts of the Lower Yangtze Valley-an index to biostratigraphy and organic

metamorphic maturity. Science Press, Beijing (in Chinese with English abstract).

Wang, C.Y., 1995a. A conodont fauna from the lowermost Kuhfeng Formation (Permian). Acta Micropalaeontologica Sinica 12, 293-297 (in Chinese with English abstract).

Wang, D.C., Jiang, H.S., Gu, S.Z., Yan, J.X., 2016. Cisuralian–Guadalupian conodont sequence from the Shaiwa section, Ziyun, Guizhou, South China. Palaeogeography Palaeoclimatology Palaeoecology 457, 1-22.

Wang, J.Z., 1995b. The "South and North Type" of the Permian Series in Hunan Province of China and Upper Permian-Lower Permian boundary in addition. Journal of Shanghai Teachers University (Natural Sciences) 24, 71-77 (in Chinese with English abstract).

Wang, W.Q., Garbelli, C., Zhang, F.F., Zheng, Q.F., Zhang, Y.C., Yuan, D.X., Shi, Y.K., Chen, B., Shen, S.Z., 2020. A high-resolution Middle to Late Permian paleotemperature curve reconstructed using oxygen isotopes of well-preserved brachiopod shells. Earth and Planetary Science Letters 540, 1-14.

Wang, X., Foster, W.J., Yan, J.X., Li, A.Z., Mutti, M., 2019. Delayed recovery of metazoan reefs on the Laibin-Heshan platform margin following the Middle Permian (Capitanian) mass extinction. Global and Planetary Change 180, 1-15.

Wang, X.D., Sugiyama, T., 2001. Middle Permian rugose corals from Laibin, Guangxi, South China. Journal Of Paleontology 75, 758-782.

Wang, Y., Jin, Y.G., 2000. Permian palaeogeographic evolution of the Jiangnan Basin, South China. Palaeogeography Palaeoclimatology Palaeoecology 160, 35-44.

Wang, Y.J., Qi, D.L., 1995. Radiolarian fauna of the Kuhfeng Formation in southern part of Jiangsu and Anhui Provinces. Acta Micropalaeontologica Sinica 12, 374-387.

Wang, Y.J., Zhang, F.F., Fan, W.M., Zhang, G.W., Chen, S.Y., Cawood, P.A., Zhang, A.M., 2010. Tectonic setting of the South China Block in the early Paleozoic: Resolving intracontinental and ocean closure models from detrital zircon U-Pb geochronology. Tectonics 29, 1-16.

Wang, Z.H., 1978. Permian-Lower Triassic condonts of the Liangshan area, southern Shannxi. Acta Palaeontologica Sinica 17, 213-231 (in Chinese with English abstract).

Wei, H.Y., Wei, X.M., Qiu, Z., Song, H.Y., Shi, G., 2016. Redox conditions across the G–L boundary in South China: Evidence from pyrite morphology and sulfur isotopic compositions. Chemical Geology 440, 1-14.

1547 Wei, H.Y., Baima, Q.Z., Qiu, Z., Dai, C.C., 2017. Carbon isotope perturbations and faunal
1548 changeovers during the Guadalupian mass extinction in the middle Yangtze Platform, South
1549 China. Geological Magazine 155, 1667-1683.
1550 Wei, H.Y., Tang, Z.W., Yan, D.T., Wang, J.G., Roberts, A.P., 2019. Guadalupian (Middle Permian)
1551 ocean redox evolution in South China and its implications for mass extinction. Chemical
1552 Geology 530, 1-14.
1553 Weidlich, O., 2002a. Permian reefs re-examined: extrinsic control mechanisms of gradual and
1554 abrupt changes during 40 my of reef evolution. Géobios 35, 287-294.
1555 Weidlich, O., 2002b. Middle and Late Permian reefs–Distributional patterns and reservoir potential,
1556 in: Kiessling, W., Fluegel, E., Golonka, J. (Eds.), Phanerozoic Reef Pattern, SEPM Special
1557 Publication No.72, pp. 339-390.
1558 Weidlich, O., Bernecker, M., 2007. Differential severity of Permian–Triassic environmental changes
1559 on Tethyan shallow-water carbonate platforms. Global and Planetary Change 55, 209-235.
1560 Wignall, P.B., Sun, Y.D., Bond, D.P.G., Gareth, I., Newton, R.J., Stéphanie, V., Mike, W., Ali, J.R.,
1561 Lai, X.L., Shui, J.H., 2009a. Volcanism, mass extinction, and carbon isotope fluctuations in
1562 the middle permian of China. Science 324, 1179-1182.
1563 Wignall, P.B., Vedrine, S., Bond, D.P.G., Wang, W., Lai, X.L., Ali, J.R., Jiang, H.S., 2009b. Facies
1564 analysis and sea-level change at the Guadalupian–Lopingian Global Stratotype (Laibin, South
1565 China), and its bearing on the end-Guadalupian mass extinction. Journal Of the Geological
1566 Society 166, 655-666.
1567 Wignall, P.B., Bond, D.P.G., Haas, J., Wang, W., Jiang, H.S., Lai, X.L., Altiner, D., Védrine, S.,
1568 Hips, K., Zajzon, N., 2012. Capitanian (Middle Permian) mass extinction and recovery in
1569 western Tethys: A fossil, facies, and δ13C study from Hungary and Hydra Island (Greece).
1570 Palaios 27, 78-89.
1571 Woodfine, R.G., Jenkyns, H.C., Sarti, M., Baroncini, F., Violante, C., 2010. The response of two
1572 Tethyan carbonate platforms to the early Toarcian (Jurassic) oceanic anoxic event:
1573 environmental change and differential subsidence. Sedimentology 55, 1011-1028.
1574 Wu, Q., Ramezani, J., Zhang, H., Wang, T.T., Yuan, D.X., Mu, L., Zhang, Y.C., Li, X.H., Shen, S.Z.,
1575 2017. Calibrating the Guadalupian series (middle Permian) of South China. Palaeogeography
1576 Palaeoclimatology Palaeoecology 466, 361-372.

1577 Wu, Q., Ramezani, J., Zhang, H., Yuan, D.X., Erwin, D.H., Henderson, C.M., Lambert, L.L., Zhang,
1578 Y.C., Shen, S.Z., 2020. High-precision U-Pb zircon age constraints on the Guadalupian in West
1579 Texas, USA. Palaeogeography Palaeoclimatology Palaeoecology 548, 1-14.
1580 Wu, S.H., Feng, Z.Z., He, Y.B., 1994. Study on anoxic environments of Permian in the Middle and
1581 Lower Yangtze region. Acta Sedimentologica Sinica 12, 29-36 (in Chinese with English
1582 abstract).
1583 Xu, T., Wei, H.Y., Zhang, X., Geng, Z.A., Wang, J.G., 2020. Genesis of hydrothermal replaced cherts
1584 in the Middle Permian Maokou Formation: evidences from elements and silicon isotopes of
1585 brecciated cherts in Sangshuwan section, Guizhou province. Acta Petrolei Sinica 41, 446-456
1586 (in Chinese with English abstract).
1587 Yan, J.X., Meng, Q., Wang, X., Liu, Z.C., Huang, H., Chen, F.Y., Guo, Q.D., 2019. Carbonate
1588 factory and carbonate platform: Progress and prospects. Journal of Palaeogeography (Chinese
1589 Edition) 21, 232-253 (in Chinese with English abstract).
1590 Yang, J.H., Cawood, P.A., Du, Y.S., Condon, D.J., Yan, J.X., Liu, J.Z., Huang, Y., Yuan, D.X., 2018.
1591 Early Wuchiapingian cooling linked to Emeishan basaltic weathering? Earth and Planetary
1592 Science Letters 492, 102-111.
1593 Yao, Y., Yan, J.X., Li, A.Z., 2012. Sedimentary features and evolution of Mid-Permian carbonates
1594 from Laibin of Guangxi. Journal of China University of Geosciences 37, 184-194 (in Chinese
1595 with English abstract).
1596 Yin, H.F., Feng, Q.L., Lai, X.L., Baud, A., Tong, J.N., 2007. The protracted Permo-Triassic crisis
1597 and multi-episode extinction around the Permian–Triassic boundary. Global and Planetary
1598 Change 55, 1-20.
1599 Yu, W.C., Algeo, T.J., Du, Y.S., Zhang, Q.L., Liang, Y.P., 2016. Mixed volcanogenic–lithogenic
1600 sources for Permian bauxite deposits in southwestern Youjiang Basin, South China, and their
1601 metallogenic significance. Sedimentary Geology 341, 276-288.
1602 Zeng, S.M., You, W., Qin, Z.S., 2010. The later period of Early Permian–Later Permian strata in the
1603 central-western Jiangxi Province, China. Geological Bulletin of China 29, 1619-1632 (in
1604 Chinese with English abstract).
1605 Zhang, B.L., Yao, S.P., Hu, W.X., Ding, H., Liu, B., Ren, Y.L., 2019a. Development of a high-
1606 productivity and anoxic-euxinic condition during the late Guadalupian in the Lower Yangtze

region: Implications for the mid-Capitanian extinction event. Palaeogeography Palaeoclimatology Palaeoecology 531, 1-16.

Zhang, B.L., Yao, S.P., Wignall, P.B., Hu, W.X., Liu, B., Ren, Y.L., 2019b. New timing and geochemical constraints on the Capitanian (Middle Permian) extinction and environmental changes in deep-water settings: Evidence from the Lower Yangtze region of South China. Journal of the Geological Society 176, 588-608.

Zhang, B.L., Yao, S.P., Mills, B.J.W., Wignall, P.B., Hu, W.X., Liu, B., Ren, Y.L., Li, L.L., Shi, G., 2020. Middle Permian organic carbon isotope stratigraphy and the origin of the Kamura Event. Gondwana Research 79, 217-232.

Zhang, B.L., Wignall, P.B., Yao, S.P., Hu, W.X., Liu, B., 2021. Collapsed upwelling and intensified euxinia in response to climate warming during the Capitanian (Middle Permian) mass extinction. Gondwana Research 89, 31-46.

Zhang, C.C., 1997. Lithostratigraphy of Hunan Province. China University of Geosciences Press, Wuhan, Hubei (in Chinese with English abstract).

Zhang, G.J., Zhang, X.L., Li, D.D., Farquhar, J., Shen, S.Z., Chen, X.Y., Shen, Y.N., 2015. Widespread shoaling of sulfidic waters linked to the end-Guadalupian (Permian) mass extinction. Geology 43, 1091-1094.

Zhang, L.L., Zhang, N., Xia, W.C., 2007. Conodont Succession in the Guadalupian–Lopingian Boundary Interval (Upper Permian) of the Maoershan Section, Hubei Province, China. Micropaleontology 53, 433-446.

Zhou, M.F., Malpas, J., Song, X.Y., Robinson, P.T., Sun, M., Kennedy, A.K., Lesher, C.M., Keays, R.R., 2002. A temporal link between the Emeishan large igneous province (SW China) and the end-Guadalupian mass extinction. Earth and Planetary Science Letters 196, 113-122.

Zhou, Z.R., 1985. Two ecological types of Permian ammonite. Science China Earth Sciences 7, 648-657 (in Chinese with English abstract).

Zhu, H.F., Qin, D.Y., Liu, C.Z., 1989. On the origin destributive pattern and tectonic control of siliceous rocks in Gufeng and Dalong Formations, South China. Experimental Petroleum Geology 11, 341-348 (in Chinese with English abstract).